Revision 2

Word Count: 15,597 (excluding References)

FLUORINE-RICH MAFIC LOWER CRUST IN THE SOUTHERN ROCKY MOUNTAINS: THE ROLE OF PRE-ENRICHMENT IN GENERATING FLUORINE-RICH SILICIC MAGMAS AND PORPHYRY MO DEPOSITS

Joshua M. Rosera[1,2], Ryan E. Frazer[3,2], Ryan D. Mills[2], Kristin Jacob[4], Sean P. Gaynor[5,2], Drew S. Coleman[2], and G. Lang Farmer[4]

[1]U.S. Geological Survey, Geology, Energy & Minerals Science Center, Reston, VA, USA

[2]Department of Earth, Marine and Environmental Sciences, University of North Carolina at Chapel Hill, Chapel Hill, NC, USA

[3]U.S. Geological Survey, Geosciences and Environmental Change Science Center, Denver, CO, USA

[4]Department of Geological Sciences, University of Colorado, Boulder, CO, USA

[5]Department of Earth Sciences, University of Geneva, Geneva, Switzerland

ABSTRACT

Fluorine-rich granites and rhyolites occur throughout the southern Rocky Mountains, but the origin of F-enrichment has remained unclear. We test if F-enrichment could be inherited from ancient mafic lower crust by: (1) measuring amphibole compositions, including F and Cl contents, of lower crustal mafic granulite xenoliths from northern Colorado to determine if they are unusually enriched in halogens; (2) analyzing whole-rock elemental and Sr, Nd, and Pb isotopic compositions for upper crustal Cretaceous to Oligocene igneous rocks in Colorado to

evaluate their sources; and (3) comparing batch melting models of mafic lower crustal source rocks to melt F and Cl abundances derived from biotite data from the F-rich silicic Never Summer batholith. This approach allows us to better determine if the mafic lower crust was pre-enriched in F, if it is concentrated enough to generate F-rich anatectic melts, and if geochemical data support an ancient lower crustal origin for the F-rich rocks in the southern Rocky Mountains.

Electron microprobe analyses of amphibole in lower crustal mafic granulite xenoliths show they contain 0.56–1.38 wt% F and 0.45–0.73 wt% Cl. Titanium in calcium amphibole thermometry indicates that the amphiboles equilibrated at high to ultrahigh temperature conditions (805 to 940 °C), and semi-quantitative amphibole thermobarometry indicates the amphiboles equilibrated at 0.5 to 1.0 GPa prior to entrainment in magmas during the Devonian. Mass balance calculations, based on these new measurements, indicate parts of the mafic lower crust in Colorado are at least 3.5 times more enriched in F than average mafic lower crust. Intrusions coeval with the Laramide Orogeny (75 to 38 Ma) pre-date F-rich magmatism in Colorado and have Sr and Nd isotopic compositions consistent with mafic lower crust ± mantle sources, but many of these intrusions contain elevated Sr/Y compositions (>40) that suggest amphibole was a stable phase during magma generation. The F-rich igneous rocks from the Never Summer igneous complex and Colorado Mineral Belt also have Sr and Nd isotopic compositions that overlap with the lower crustal mafic granulite xenoliths, but they have lower Sr/Y, higher Nb and Y abundances, and distinctly less radiogenic $^{206}Pb/^{204}Pb_i$ compositions than preceding Laramide magmatism. Batch melt modeling indicates low-degree partial melts derived from rocks similar to the mafic lower crustal xenoliths we analyzed can yield silicic melts with

>2000 ppm F, similar to estimated F melt concentrations for silicic melts that are interpreted to be parental to evolved leucogranites.

We suggest that F-rich silicic melts in the southern Rocky Mountains were sourced from garnet-free mafic lower crust, and that fluid-absent breakdown of amphibole in ultrahigh temperature metamorphic rocks was a key process in their generation. Based on the composition of high-F amphibole measured from lower crustal xenoliths, the temperature of amphibole breakdown and melt generation for these F-enriched source rocks is likely >100 °C greater than similar lower crust with low or average F abundances. As such, these source rocks only melted during periods of unusually high heat flow into the lower crust, such as during an influx of mantle-derived magmas related to rifting or the post-Laramide ignimbrite flare-up in the region. These data have direct implications for the genesis of porphyry Mo mineralization, because they indicate that pre-enrichment of F in the deep crust could be a necessary condition for later anatexis and generation of F-rich magmas.

Keywords: fluorine, amphibole, Climax-type Mo deposits, topaz rhyolite, xenolith, southern Rocky Mountains, ultrahigh temperature metamorphism, granulite

INTRODUCTION

Fluorine-rich granites and rhyolites are often associated with economic mineral deposits of Sn, W, Be, U, F, Mn, Y, and REEs (e.g., Burt et al. 1982; Carten et al. 1993; Lüders et al. 2008; Dostal et al. 2016; Liu et al. 2016; O'Neill et al. 2017; Dailey et al. 2018; Girei et al. 2020; Hofstra and Kreiner 2020). Numerous Mo-producing mines in the western United States are also associated with F-rich granites ("Climax-type" deposits; Ludington and Plumlee 2009), and therefore there is considerable interest in exploring the origin and distribution of F-rich granitic

systems. The mineralizing intrusions in Climax-type deposits are often highly silicic (>75 wt% SiO_2), slightly peraluminous, enriched in incompatible elements (e.g., Nb, Y, Rb), and depleted in elements compatible in feldspar (Sr, Ba, Eu^{2+}; Carten et al. 1993; Ludington and Plumlee 2009). These mineralizing intrusions are also chemically similar to topaz rhyolites and topaz granites (Christiansen et al. 2007; Jacob et al. 2015). At least three Climax-type deposits, including the eponymous Climax mine (Colorado), Henderson deposit (Colorado), and the Pine Grove deposit (Utah), are directly associated with topaz rhyolite eruptions (Keith et al. 1986; Bookstrom 1989; Mercer et al. 2015). Topaz rhyolites, unmineralized topaz granites, and the mineralizing intrusions in Climax-type deposits all form in tectono-magmatic environments in which ferroan silicic magmas are commonly generated (e.g., Christiansen et al. 2007; Frost and Frost 2011; Jacob et al. 2015).

The origins of F-rich melts in porphyry Mo deposits and related systems are unclear despite decades of research (e.g., White et al. 1981; Christiansen et al. 1983; Farmer and DePaolo 1984; Clemens et al. 1986; Carten et al. 1988; Stein and Crock 1990; Christiansen et al. 2007; Audétat and Li 2017). Audétat (2015) suggested F-rich granites and rhyolites could form by low-degree partial melting of F-rich sources. However, it is not clear which, if any, specific source rocks are ultimately responsible for generating F-rich mineralizing intrusions. Some models suggest that F-rich silicic melts are produced by anatexis of felsic or mafic granulites in the lower crust (Stein and Crock 1990; Skjerlie and Johnston 1993; Jacob et al. 2015), whereas others suggest that silicic melts associated with large porphyry Mo deposits are derived by differentiation of melts extracted from metasomatized lithospheric mantle (Pettke et al. 2010; Liu et al. 2019). It is also unclear whether the high F abundances (>2000 ppm) in these silicic igneous rocks are inherited from their melt source or are introduced externally. For example,

topaz rhyolites and Climax-type intrusions are often part of bimodal magma suites (Christiansen et al. 2007; Ludington and Plumlee 2009), and therefore it is possible that the halogens are introduced into silicic magmas by fluids exsolved from crystallization of mafic magmas that intrude the bases of upper crustal silicic magma bodies, or during deep crustal hybridization related to intrusion of mantle-derived magmas (e.g., Rosera et al. 2013; Dailey et al. 2018).

Disentangling the origins of the silicic melts and whether F and Cl are introduced externally is challenging because the hypothesized processes responsible for their origin extend from deep to shallow crust. Trace element geochemistry and Sr, Nd, and Pb isotopic compositions are one method to explore sources of magmatism, but they still require some knowledge about the composition of deep crust or the lithospheric mantle. Early isotopic studies that explored the origin of F-rich granites and rhyolites in the western United States (e.g., Farmer and DePaolo 1984; Stein and Crock 1990) were conducted before isotopic compositions of lower crustal xenolith suites in the region were fully characterized (e.g., Selverstone et al. 1999; Farmer et al. 2005). Furthermore, early studies suggested basaltic end members to magma systems were sourced from depleted mantle, whereas other studies document evidence that large portions of the western United States contain enriched lithospheric mantle (e.g., Coleman et al. 1992; Pettke et al. 2010; Sun et al. 2021). A more comprehensive examination of lower crustal xenolith data, as well as trace element and isotope geochemistry, is required to characterize sources of F-rich granites and rhyolites in the western United States.

The Colorado Mineral Belt is a narrow region of Late Cretaceous and younger (approximately 75 to 5 Ma) intrusions and mineral deposits that trends southwest-northeast across the southern Rocky Mountains of Colorado (Fig. 1a). This area provides an exceptional opportunity to test hypotheses related to the origin of F-rich, highly silicic magmas because it

hosts numerous Climax-type deposits and porphyry Mo prospects (Fig. 1a), as well as topaz rhyolites and fluorite-bearing leucogranites. This study tests inferences regarding the origins of F-rich magmas by several avenues. To determine whether mafic lower crust is a viable source for F-rich silicic melts, we measure halogen abundances of the mafic lower crust beneath the Colorado Mineral Belt region as sampled by local kimberlite-borne crustal xenoliths. We combine this information with estimated F and Cl concentrations in melt from an F-rich granite porphyry in the bimodal Never Summer batholith in northern Colorado, which is outside of the Colorado Mineral Belt as traditionally defined (e.g., Tweto and Sims 1963; Chapin, 2012), but contains granite that is temporally and chemically similar to Mo-mineralizing intrusions in the Colorado Mineral Belt. We also use whole-rock major, trace, and isotopic compositions (Sr, Nd, and Pb) from fifty-six new samples to assess the sources of F-rich silicic magmatism in the region and to place them within the greater context of Cenozoic magmatism in Colorado. Ultimately, these data provide a clearer picture of the processes that aligned to set the stage for generating Climax-type mineral systems.

GEOLOGICAL SETTING

Cretaceous to Oligocene magmatism in central and northern Colorado

Cretaceous to Oligocene igneous rocks in central and northern Colorado have been a topic of interest for over a century because they represent magmatism that developed deep within a continental interior, and because of their close spatial relationship to numerous mining districts throughout the state (Emmons 1886; Tweto and Sims 1963; Bookstrom 1990; Chapin 2012; Rosera et al. 2021). The igneous rocks in the region have been classified by numerous schemes, such as compositional or spatial groups, especially in the Colorado Mineral Belt (e.g., Simmons and Hedge 1978; Mutschler et al. 1987; Stein and Crock 1990). However, we have chosen to

broadly group them into temporal tectono-magmatic suites: 1) Laramide: those broadly associated with Laramide-aged compression (approximately 75 to 38 Ma; Chapin 2012); 2) transitional: rocks that originated during a post-orogenic period when compression relaxed, but before major tectonic extension (ca. 38 to 30 Ma; Zimmerer and McIntosh 2012); and 3) extensional: rocks generated after initiation of significant extension in the region, including development of the Rio Grande Rift (after ca. 30 Ma; Table 1; Chapin 2012; Landman and Flowers 2013).

Laramide compression.

Shallow subduction of a thickened segment of the Farallon plate is suggested to have caused widespread deformation and uplift in southwestern North America during the Laramide orogeny (Erslev 2005; Jones et al. 2011). Continental magma systems were also active in Idaho, southern Arizona and southwestern New Mexico between approximately 75 to 40 Ma. The region extending from central New Mexico through Wyoming largely lacked significant magmatism, with the exception of the Colorado Mineral Belt, which occupied this broad magmatic gap (Fig. 1a; Jones et al. 2011). Most Laramide-age rocks exposed in the Colorado Mineral Belt are shallow intrusions and porphyries; penecontemporaneous volcanic rocks are volumetrically minor and mostly preserved in uplift-flanking basins (Tweto 1975). Intrusive rocks include alkaline plutons ("monzonite suite" of Simmons and Hedge 1978) and a much more voluminous suite of calc-alkaline rocks (quartz monzonites to granodiorite). The calc-alkaline suite has higher initial $^{87}Sr/^{86}Sr$ ($^{87}Sr/^{86}Sr_{i,}$ 0.706 to 0.7089) and slightly lower initial εNd (εNd_i, -5 to -10) compared to alkaline rocks ($^{87}Sr/^{86}Sr_i$ mostly <0.706, εNd_i -1 to -9; Table 1) . Both suites have broadly been interpreted to be sourced from mafic lower crust (Simmons and Hedge 1978; Stein and Crock 1990). In the northeastern Colorado Mineral Belt, alkaline magmas

158 are associated with Au, Ag, U, W, and Te mineralization in the form of stockworks and veins
159 (Bookstrom 1990). Calc-alkaline magma systems that intruded between approximately 45 to 38
160 Ma are genetically associated with intermediate sulfidation veins, stockwork, and carbonate-
161 replacement deposits that were mined mainly for Pb-Zn-Ag in districts such as Montezuma,
162 Breckenridge and Leadville (Fig. 1c; Bookstrom 1990; Rosera et al. 2021).

163 **Transitional.**

164 A shift in the tectono-magmatic framework for the region occurred near the end of the
165 Eocene. We use the eruption of the 37.3 Ma Wall Mountain Tuff to mark the beginning of this
166 transitional period (Rosera et al. 2021), as the supereruption of this tuff signaled the start of an
167 ignimbrite flare-up and deposition of voluminous volcanic material in the Southern Rocky
168 Mountain volcanic field (McIntosh and Chapin 2004; Lipman 2000; Lipman 2007; Farmer et al.
169 2008). The Mount Princeton batholith, as well as the Mount Aetna and Grizzly Peak calderas,
170 formed early in this time frame (Fig. 1c; Fridrich et al. 1998; Mills and Coleman 2013). Low-
171 grade porphyry Mo deposits also formed during this interval, including those at Turquoise Lake,
172 Middle Mountain, and Halfmoon Creek (Van Loenen et al. 1989; Rosera et al. 2021; Fig. 1c).
173 The flare-up has been suggested to have been triggered by exposing relatively cold
174 metasomatized lithospheric mantle of the North American lithosphere to hot asthenosphere
175 following fragmentation and foundering of the Farallon plate near the end of the Laramide
176 (Dumitru et al. 1991; Humphreys et al. 2003; Farmer et al. 2008, 2020).

177 **Extensional.**

178 The tectonic environment evolved towards continental extension and initial Rio Grande
179 rift development around approximately 30 to 25 Ma (Tweto 1979; Landman and Flowers 2013;
180 Abbey and Niemi 2020). Broadly north-south elongated rift-related basins terminate near

Leadville in the central Colorado Mineral Belt, but major Neogene faults concurrent with rift subsidence extend from the central Colorado Mineral Belt through the Never Summer range near the Wyoming-Colorado border (Tweto 1979; Fig. 1). Magmatism associated with extension began as early as ca. 31 to 28 Ma, when F-rich leucogranites intruded at Mount Antero and in the Never Summer mountains (Fig. 1b; Zimmerer and McIntosh 2012; Jacob et al. 2015; Rosera et al. 2021). Large Mo-F deposits at Climax and Henderson were assembled after extension began (Carten et al. 1993; Ludington and Plumlee 2009), along with eruption of numerous topaz rhyolites (Christiansen et al. 2007). High-silica rocks in this "extensional suite" are often interpreted to have been sourced from intermediate to felsic crust, owing to their generally low εNd_i and slightly elevated $^{87}Sr/^{86}Sr_i$ relative to older igneous rocks from the Laramide and post-Laramide transition (Farmer and DePaolo 1984; Stein and Crock 1990; Table 1), although some high-silica magmas may have been derived from mafic lower crust (e.g., the Never Summer batholith; Jacob et al. 2015).

The Never Summer batholith is the most voluminous bimodal intrusive center that formed during early stages of extension in Colorado and is composed of the Mount Richthofen and Mount Cumulus plutons (Fig. 1b). The oldest intrusive rocks in the system are 29.21 Ma rhyolite porphyry dikes that intruded dominantly Paleozoic-Mesozoic sedimentary rocks in the northern portion of the igneous complex (Fig. 1b; Rosera et al. 2021). These silicic dikes contain quartz, K-feldspar, and plagioclase phenocrysts, and mafic phenocrysts that are largely altered to chlorite. The 28.98 to 28.74 Ma Mount Richthofen pluton is a compositionally heterogenous granodiorite with SiO_2 contents ranging from 55 to 67 wt%, and it is interpreted to have formed by mixing of mantle-derived mafic melts with crustally-derived silicic melt (Jacob et al. 2015). Quartz, orthoclase, plagioclase, amphibole, and biotite are present throughout the Mount

Richthofen pluton. Biotite tends to be the more dominant mafic mineral phase in the silicic portions of the pluton, and amphibole (±clinopyroxene) is more abundant in mafic portions of the pluton (Jacob et al. 2015). The younger Mount Cumulus pluton (28.17 Ma; Rosera et al. 2021) is composed of a fluorite-bearing granite porphyry with major and trace element abundances comparable to that of the topaz rhyolites and intrusions in Climax-type deposits (Jacob et al. 2015). Biotite is the dominant mafic mineral phase in the Mount Cumulus pluton. High-precision U/Pb zircon geochronology indicates that the Mount Cumulus pluton was assembled rapidly, over 10's to 100's of k.y (Rosera et al. 2021). The Never Summer batholith is not significantly mineralized, but an area west of Mount Cumulus was prospected for porphyry Mo mineralization (Pearson et al. 1981). Molybdenite was also reported to occur in miarolitic cavities in the Mount Cumulus pluton, and rock chip surveys identified anomalously high abundances of Mo and Ag (Pearson et al. 1981).

Lower crustal mafic granulite xenoliths

The State Line district of xenolith-bearing kimberlite dikes and diatremes located near the Colorado-Wyoming border intruded in two episodes during the Neoproterozoic and in the Devonian (Lester and Farmer 1998; Fig. 1a). Thus, these xenoliths sampled northern Colorado lithosphere before inferred Laramide aqueous metasomatism and magmatism. Xenoliths are predominantly mafic granulites and broadly include garnet-bearing and garnet-free groups. Garnet-free samples contain locally abundant amphibole (up to 30 modal %), plagioclase, clinopyroxene and orthopyroxene (Fig. S1), as well as trace to minor quartz, alkali feldspar, biotite, rutile, ilmenite, zircon, and apatite (Bradley 1985). The variable mineralogy of the xenoliths has been interpreted to reflect equilibration of compositionally similar rocks over a range of mid- to lower-crustal temperature and pressure conditions (Bradley and McCallum

1984; Bradley 1985). Whole-rock major and trace element abundances, as well as H_2O concentrations in nominally anhydrous minerals, indicate that the protolith for the State Line granulite suite was a hydrous (>1 wt% H_2O) mafic igneous rock that intruded the deep crust (Farmer et al. 2005; Chin et al. 2020). Zircon U/Pb geochronology indicates primary igneous crystallization occurred at approximately 1720 Ma, but a subset of approximately 1360 Ma zircons showed sector zoning in cathodoluminescence images were interpreted as metamorphic overprint (Farmer et al. 2005). Garnet-pyroxene-plagioclase equilibria indicate that the garnet-bearing assemblage of xenoliths range from 1.1–1.2 GPa and 700–800 °C (Farmer et al. 2005). Thermobarometry estimates for the garnet-free suite of State Line mafic granulite xenoliths have not been previously published.

RESULTS

We use electron microprobe analyses (EMPA) of amphibole in garnet-absent two-pyroxene granulite xenoliths from the Sloan and Nix diatreme pipes from the State Line district to derive a first-order estimate of halogen contents of the garnet-free mafic lower crust from which they were derived (Fig. 1a). Fluorine and Cl occur in limited to trace quantities in apatite and nominally anhydrous minerals in the garnet-bearing granulite xenoliths because amphibole is absent. Consequently, no garnet-bearing xenoliths were used in this study. We also analyzed biotite in five samples from the Never Summer batholith: two from the Mount Richthofen pluton and three from the fluorite-bearing Mount Cumulus pluton (all samples used for biotite EMPA are from Jacob et al. [2015], except for sample NS17-05; Fig. 1b). We focused on biotite because amphibole is absent in the Mount Cumulus pluton, and biotite occurs in much greater abundance than amphibole in the silicic portions of the Mount Richthofen pluton (Jacob et al. 2015). The mafic portion of the Mount Richthofen pluton contains both amphibole and biotite, but

amphibole from this sample were analyzed previously by Jacob et al. (2015; sample 10-KJ-MR-109). We used the same sample to measure biotite compositions.

We measured major and trace element abundances, as well as isotopic compositions of Sr, Pb, and Nd, on fifty-six whole-rock samples (further whole rock sample details and analytical methods are presented in the Supporting Information, Text S1 and S2). Samples were selected to: 1) cover the temporal (Cretaceous to Oligocene) and spatial (northern and central Colorado Mineral Belt, Never Summer batholith) range of calc-alkaline magmatism (Fig. 1), and 2) add sampling density to previously studied systems (e.g., Montezuma pluton; Twin Lakes pluton; Farmer and DePaolo 1984; Stein and Crock 1990). This approach allows us to detect spatial and temporal variations in the sources of magmatism in order to better place the origins of F-rich magmatism into the greater context of regional magmatism. Laramide-aged (75 to 38 Ma) intrusions were collected from the Montezuma, Breckenridge, Alma, Leadville, and the Twin Lakes areas (Fig. 1). Samples corresponding to a transitional period between Laramide compression and Rio Grande rift extension (38 Ma to about 31 Ma) were collected from the Sawatch Range, and include the Mount Princeton batholith, Grizzly Peak caldera, and porphyritic intrusions related to Mo prospects (Turquoise Lake and Middle Mountain). Finally, we collected numerous samples from units that formed after the start of Rio Grande rift extension, including the Chalk Mountain rhyolite that is directly related to the Climax porphyry Mo deposit (Bookstrom 1989; Audétat 2015), Mount Antero leucogranites, and the silicic end member of the Never Summer batholith (Jacob et al. 2015).

This is the peer-reviewed, final accepted version for American Mineralogist, published by the Mineralogical Society of America.
The published version is subject to change. Cite as Authors (Year) Title. American Mineralogist, in press.
DOI: https://doi.org/10.2138/am-2022-8503. http://www.minsocam.org/

Electron microprobe analysis

Normalization procedures.

Normalization of electron microprobe data for biotite and amphibole can be complicated because: 1) analyses cannot detect the incorporation of anhydrous O^{2-} into W crystallographic sites that are usually occupied by OH, F, and Cl; and 2) it does not provide information about oxidation states, which is problematic for major elements with multiple common oxidation states, most notably Fe (i.e., Fe^{3+} or Fe^{2+}). Normalization schemes for EMPA data from biotite and amphibole therefore require defining a set of assumptions or normalization scenarios to estimate O^{2-} and Fe^{3+}/Fe_{total}. We note that the normalization procedures of EMPA data for estimating Fe^{3+} and O^{2-} in biotite and amphibole are not ideal, but they are considered more accurate than assuming: 1) that $Fe^{3+}/Fe_{total} = 0$ (e.g., Hawthorne et al. 2012), or that 2) there is no anhydrous O in the W crystallographic site for these minerals, especially those that have abundant Ti (e.g., Hawthorne et al. 2012).

The incorporation of anhydrous O into the W sites of amphibole and biotite has been interpreted to be due to deprotonation related to Ti substitution, such as $(Fe^{2+}, Mg) + 2OH^- = Ti^{4+} + 2O^{2-}$ (Oberti et al. 1992; Henry et al. 2005). Consequently, the maximum abundance of anhydrous O can be calculated as $O^{2-} = 2Ti^{4+}$ (e.g., Hawthorne et al. 2012; Henry and Daigle 2018). In this study, we use these Ti substitution formulations to estimate O^{2-} occupancy in the W crystallographic sites for biotite and amphibole, and we normalize biotite to $11O + 2^{W}(OH, F, Cl, O)$ and amphibole to $22O + 2^{W}(OH, F, Cl, O)$.

The Fe^{3+}/Fe_{total} value for biotite and amphibole can be estimated based on independent lines of evidence, or by using a cation normalization scheme and adjusting Fe^{3+} to maintain electroneutrality. For amphibole analyses, we averaged Fe^{3+}/Fe_{total} based on the 13-cation (i.e., Si

through Mg) and 15-cation (Si through Ca) schemes using software from Locock (2014). For biotite from the Never Summer batholith, we assumed $Fe^{3+/}Fe_{total} = 0.22$ based on the presence of magnetite throughout the system (Guidotti and Dyar 1991; Jacob et al. 2015; Fig. S2), which is within uncertainty of $Fe^{3+/}Fe_{total}$ measured independently in biotite from the Mount Princeton quartz monzonite and Mount Antero leucogranite in the central Colorado Mineral Belt ($Fe^{3+/}Fe_{total} = 0.18 \pm 0.06$, 1σ; Toulmin and Hammarstrom 1990).

Amphibole compositions and thermobarometry.

Amphibole in the State Line mafic granulite xenoliths are mainly potassic-pargasite to potassic-magnesio-hastingsite. Sample SD2-LC76 contains potassic-fluoro-pargasite (*i.e.*, F > OH; Hawthorne et al. 2012). Fluorine concentrations for all amphibole analyzed range from 0.56 to 1.38 wt% F, corresponding to 0.27 and 0.67 F atoms per formula unit (apfu; Fig. 2 and Table S1). Chlorine concentrations range from 0.45 to 0.73 wt% Cl (0.12 to 0.19 apfu Cl) and broadly show a positive correlation with F (Fig 2b). Samples NX4-LC2 and SD2-LC76 contain Ti-rich amphibole (0.5 > Ti > 0.3 apfu; Hawthorne et al. 2012). The entire amphibole data set has relatively limited ranges of Mg# (0.53 to 0.60), Si (5.97 to 6.28 apfu), Ca (1.79 to 1.97 apfu), and ^{IV}Al (1.72 to 2.03 apfu; Fig. 2; Table S1).

The presence of ilmenite and rutile in the two-pyroxene mafic granulite xenoliths permits use of a recently calibrated Ti in calcium amphibole thermometer (Liao et al. 2021). This thermometer has a reported precision of approximately ± 35 °C (Liao et al. 2021). We compare those data to a graphical, semiquantitative Al_2O_3-TiO_2 amphibole thermobarometer calibrated for basaltic protoliths by Ernst and Liu (1998). Hence, we estimate both the *T* and *P* equilibration conditions for amphibole in the xenolith samples, but it should be noted that the *P* estimates are derived from a semiquantitative method for which fully propagating errors is difficult.

316 Amphibole in sample SD2-LC78 is compositionally distinct from amphibole in the other
317 xenoliths (Fig. 2), and application of the Ti in calcium amphibole thermometer yields
318 equilibration temperatures from 805 to 870 °C (Fig 3). This temperature estimate is slightly
319 lower, but overlapping, temperature estimates from the semiquantitative thermobarometer of
320 Ernst and Liu (1998), which yielded equilibration conditions between approximately 820 and
321 880 °C and approximately 0.5–0.75 GPa (Fig. 3). The remaining samples all contain amphibole
322 with greater abundances of F, K, Ti, and ^{IV}Al than those in SD2-LC78 (Fig. 2), and they yielded
323 equilibration temperatures from 873 to 941 °C using the Ti in calcium amphibole thermometer.
324 These temperature estimates overlap those from the semiquantitative method, which yielded
325 values ranging from 870 to 940 °C, and an estimated equilibration pressure of 0.6 to ~1.0 GPa.
326 These pressure estimates are lower than peak metamorphic conditions calculated for the garnet-
327 pyroxene-plagioclase xenoliths from the State Line district, but the temperature estimate is up to
328 140 °C hotter than peak conditions estimated by Farmer et al. (2005; Fig. 3).

329 **Biotite from the Never Summer batholith.**

330 Biotite was analyzed in five samples from the Oligocene Never Summer batholith.
331 Biotite from two samples of the Mount Richthofen pluton were analyzed: one from the mafic end
332 member (~55 wt% SiO_2) and another from a more silicic sample (~64 wt% SiO_2; Jacob et al.
333 2015). Biotite from these two samples have total Al and $Fe^{2+}/(Fe^{2+} + Mg)$ values comparable to
334 biotite from the Mount Princeton and Mount Antero system in the Colorado Mineral Belt
335 (Toulmin and Hammarstrom 1990; Fig. 4a). Biotite from the mafic portion of the Mount
336 Richthofen pluton has slightly lower $X_{phlogopite}$ (0.46–0.48; $X_{phlogopite}$ in this study is defined as
337 $Mg/[Mg + {}^{VI}Al + Cr + Ti + Fe^{2+} + Fe^{3+} + Mn]$) than those analyzed from the silicic portion of the
338 pluton ($X_{phlogopite}$: 0.49–0.52; Fig. 4b). The more silicic sample yielded biotite with higher

339 log(F/OH) values (-0.83 to 0.74) and lower log(Cl/OH) (-1.88 to -1.68) than biotite from the
340 mafic sample (log(F/OH): -1.29 to -1.24; log(Cl/OH): -1.49 to -1.43; Fig. 4b,d). Biotite from the
341 silicic portion of the Mount Ricthofen pluton have higher Ti abundances than those in the more
342 mafic sample (Fig. 4c). Biotite equilibration temperatures were estimated with the Ti in biotite
343 geothermometer of Henry et al. (2005) and yielded equilibration temperatures of approximately
344 730˚C for the mafic sample, and 765 to 780˚C for the silicic portion of the Mount Richthofen
345 pluton (Fig. 4c, Table S2).

346 Mount Cumulus samples contain two petrographically and compositionally distinct types
347 of biotite. The first group occurs in samples 10-KJ-MC-94 and 10-KJ-MC-91 from the eastern
348 and central portion of the pluton, respectively (Fig. 1b) and is commonly associated with fluorite
349 and zircon (Fig. S2c). Compositionally, these biotite have very low $X_{phlogopite}$ components (< 0.03
350 apfu), high siderophyllite components (Al_{total}: 1.59 to 1.67 apfu), high log(F/OH) (0.13 to 0.35)
351 and correspondingly high F concentrations (3.9 to 4.8 wt%; Fig. 4a,d, Table S2). Log(Cl/OH)
352 values for these biotite span a relatively large range (-1.34 to -1.02; Fig. 4b). The low Mg
353 abundances for these biotite are outside of the calibration range for the Ti in biotite
354 geothermometer of Henry et al. (2005), and the Ti abundances are the lowest we observed the
355 Never Summer batholith (0.09 to 0.11 apfu; Fig. 4c).

356 Biotite in a sample from the western portion of the pluton near Baker Pass (NS17-05) are
357 petrographically and compositionally distinct from Fe-rich biotite observed in the other two
358 Mount Cumulus samples. Fluorite was not observed in sample NS17-05, and some biotite in this
359 sample encloses and cuts Fe-Ti oxide clusters (Fig. S2d). Compositionally, biotite in this sample
360 contain higher $X_{phlogopite}$ (0.27 to 0.30), log(Cl/OH) (-1.27 to -1.10) and lower Al_{total} (1.13 to 1.24
361 apfu) and log(F/OH) (-0.29 to 0.06) than the other Mount Cumulus samples (Fig. 4). Titanium

362 abundances in these biotite are intermediate between the other Mount Cumulus samples and
363 biotite from the Mount Richthofen pluton, corresponding to estimated equilibration temperatures
364 from 639 to 653 ˚C (Henry et al. 2005; Fig. 4c).

365 **Whole-rock geochemistry of Cretaceous to Oligocene rocks**

366 **Laramide compressional suite.**

367 Analyzed samples of intrusive rocks associated with Laramide compression contain 48 to
368 78 wt% SiO_2, are mostly slightly peraluminous, and range from magnesian to ferroan (Fig. 5).
369 Strontium abundances broadly follow a flat log-linear relationship with SiO_2 (>400 ppm Sr),
370 except in the most silicic samples that are Sr-depleted (>75 wt% SiO_2; Fig. 6a). Rubidium, Nb,
371 Y, and Rb/Sr values for the Laramide suite are low relative to younger rocks from transitional
372 and extensional suites (Fig. 6b-e), except for a modally layered mafic rock from the Twin Lakes
373 pluton (SiO_2 = 48 wt%), which contains greater abundances of Nb and Y. The Laramide suite
374 includes samples with high Sr/Y (>40) values, most notably those from the Twin Lakes pluton
375 and intermediate intrusions from the Breckenridge, Alma, and Leadville mining districts (Fig.
376 6f).

377 The Laramide suite of rocks show little correlation between initial isotopic compositions
378 of Pb, Sr, and Nd relative to silica content (Figs. 7-9). Samples from this suite plot near or below
379 the Stacey and Kramers (1975) two-stage Pb growth curve in $^{206}Pb/^{204}Pb$-$^{207}Pb/^{204}Pb$ space, and
380 slightly above the $^{206}Pb/^{204}Pb$-$^{208}Pb/^{204}Pb$ curve (Fig. 7b,d). Initial $^{206}Pb/^{204}Pb$ compositions of
381 the Twin Lakes pluton are similar to intermediate intrusions from the Breckenridge, Alma, and
382 Leadville areas, whereas samples from Montezuma are more enriched in $^{206}Pb/^{204}Pb$ (Fig. 7;
383 Table S5). Initial $^{87}Sr/^{86}Sr$ is not correlated with SiO_2 and generally increases from <0.707 in the
384 southwest (Twin Lakes pluton) to 0.708 to 0.712 in the northeast (Montezuma mining district;

Fig. 8; Table S6). Initial εNd values for the Twin lakes pluton and intrusions from the Montezuma district are similar and generally yield εNd_i near -8, except for a late trachyandesite dike that cuts the Montezuma pluton, which has εNd_i = -6.4 (Fig. 9; Table S6). Samples from intrusions around the Breckenridge, Alma, and Leadville mining districts yielded εNd_i values between -11.1 to -5.9, with the lowest value being from a xenolith entrained in the younger Chalk Mountain topaz rhyolite (CMR16-01x; Table S6), and the highest from the Swan Mountain sill complex near Breckenridge.

Transitional suite.

Igneous rocks from the transitional suite are metaluminous to slightly peraluminous and generally contain higher total alkali contents than those from the older Laramide suite (Fig. 5). Values of Rb/Sr, Nb, Y, and Nb for samples from the transitional suite are similar to the Laramide suite. Strontium and Sr/Y values are mostly lower than those from the Laramide suite (i.e., lower than those from the Twin Lakes pluton and Breckenridge, Alma, and Leadville areas; Fig. 6a, f).

Samples from the transitional suite generally yield wider ranges in initial isotopic compositions of Pb, Sr, and Nd than the Laramide suite. Samples related to porphyry Mo prospects at Turquoise Lake and Middle Mountain yield relatively high $^{208}Pb/^{204}Pb_i$ values relative to $^{206}Pb/^{204}Pb_i$ and plot near the continental lithospheric mantle (CLM) Pb growth curve for the western United States proposed by Pettke et al. 2010 (Fig. 7d). Initial Pb and Sr isotope compositions do not vary relative to silica content, but they do vary between individual magma systems (i.e., Grizzly Peak caldera system relative to the Mount Princeton batholith; Figs. 6, 7). Samples from the Grizzly Peak caldera complex yield a slight negative correlation between εNd_i and SiO_2, and contain the lowest εNd_i in the central Colorado Mineral Belt (-14.6 to -8.5; Fig. 9;

Table S6). Samples from the Mount Princeton batholith and porphyry Mo prospects at Turquoise Lake and Middle Mountain yield more radiogenic εNd_i values (-10.5 to -8.7; Fig. 9).

Extensional suite.

Ten samples analyzed belong to the <31 Ma extension suite. One sample is a mafic volcanic rock located in the Rio Grande Rift (SiO_2 = 59 wt%), and the other samples are all rhyolites or granites (SiO_2 > 71 wt%). The silicic samples from the extensional suite are slightly peraluminous and ferroan (Fig. 5) and yield higher values of Nb, Y, and Rb/Sr than the majority of samples from the transitional or Laramide suites (Fig. 6). Strontium abundances are mostly <200 ppm, and Sr/Y values are correspondingly low (<10; Fig. 6a, f).

Samples from the extensional suite yielded initial widely variable Pb, Sr, and Nd isotopic compositions. The samples from the Never Summer igneous complex are more radiogenic in terms of Pb, Sr, and Nd (Figs. 7-9). Extensional suite rocks from the Colorado Mineral Belt have relatively unradiogenic Pb isotopic compositions (Fig. 7) and intermediate Sr and Nd isotopic compositions relative to the transitional and Laramide suites (Figs. 8, 9). The Chalk Mountain rhyolite erupted from the magma system that formed the Climax Mo deposit (Bookstrom et al. 1987), and the sample we analyzed yielded Pb, Sr, and Nd compositions comparable to mineralizing intrusions from the mine (Figs. 7-9; Stein 1985; Stein and Crock 1990).

DISCUSSION

Interpretation of amphibole data from mafic granulite xenoliths

Characterization of amphibole in the State Line xenoliths.

Bradley (1985) concluded that amphibole in the two-pyroxene granulites from the State Line district was in equilibrium with surrounding minerals. We observed numerous K-feldspar

and barite rims and veinlets in the State Line xenoliths but found no significant core-to-rim variations in K abundances across amphibole crystals. Petrography and backscattered electron imagery indicate that plagioclase is variably altered to sericite in some of the samples we analyzed (Fig. S1), but amphibole appears unaffected (Fig. 10). There is no obvious correlation between the alteration intensity of feldspar and amphibole compositions within the samples studied. Therefore, we conclude the amphibole crystals we analyzed are unaffected by alteration from the kimberlite host rock.

There is a weak positive correlation between Cl and $Fe^{2+}/(Fe^{2+} + Mg)$ in amphibole from the xenoliths (Fig. 2c). This is consistent with the Mg-Cl avoidance principle (or Fe-F avoidance) in amphiboles and micas (Rosenberg and Foit 1977; Munoz 1984). The avoidance of Mg-Cl and Fe-F is potentially related to variations in bonding strength, wherein Fe cations create weaker bonds with F in amphibole than Mg cations (Rosenberg and Foit 1977). As a result, the ability of amphibole or biotite to incorporate F and Cl into their crystal structure is, in part, a function of Mg and Fe concentrations (e.g., Munoz 1984). Although we observe slight negative correlation between Cl and Fe in amphibole from the State Line xenoliths, the relatively poor correlation suggests other factors beyond amphibole composition also influenced halogen abundances (e.g., Morrison 1991; Aranovich and Safonov 2018).

P-T equilibration conditions.

Mafic lower crustal xenoliths from the Leucite Hills (Wyoming) and the Four Corners area of the Colorado plateau (Fig. 1a) yield equilibrium pressure estimates similar to the State Line xenoliths (0.8–1.2 GPa; Selverstone et al. 1999; Farmer et al. 2005). However, amphiboles from most State Line mafic granulite xenoliths have higher concentrations of K, Ti and ^{IV}Al than those observed in otherwise similar western U.S. xenoliths, corresponding to higher equilibration

453 temperatures at a given pressure (Spear 1981; Fig. 2). The high Ti and ^{IV}Al abundances in
454 amphibole from the State Line xenoliths are similar to fluorian pargasite in the ultrahigh
455 temperature (UHT) Highland Complex in Sri Lanka (Fig. 2e; Sajeev et al. 2009), and Ti in
456 calcium amphibole thermometry also indicate that amphibole in some of the State Line mafic
457 granulite xenolith samples equilibrated at temperatures greater than 900 °C (Fig. 3). Fluorine-
458 rich pargasite is stable at more extreme *P-T* conditions than its F-poor counterparts because
459 substitution of F into the hydroxyl site expands pargasite's thermal stability field (up to 950 °C at
460 1.0 GPa; Holloway and Ford 1975; Tsunogae et al. 2003; Sajeev et al. 2009). The high F and Cl
461 concentrations observed in State Line amphibole could therefore stabilize mafic lower crust and
462 allow it to equilibrate at temperatures in excess of 800°C without significant dehydration or
463 partial melting.

464 Altogether, the observations of granulite textures in the mafic lower crustal xenoliths
465 (Bradley 1985; Farmer et al. 2005; Chin et al. 2020; Fig. S1), as well as amphibole compositions
466 and Ti in calcium amphibole data presented here, strongly suggest that portions of the mafic
467 lower crust of northern Colorado were subjected to high or UHT (>900 °C) peak metamorphic
468 conditions. The temperature estimates for the garnet-absent mafic crust are greater than those
469 from the deeper-sourced garnet-bearing xenoliths measured by Farmer et al. (2005; Fig. 3),
470 suggesting that either some high-T process overprinted the shallower garnet-absent lower crust,
471 or perhaps the lowermost garnet-bearing crust formed by a retrograde reaction beginning with
472 amphibole-bearing garnet-absent granulite. The latter model seems unlikely, because
473 disequilibrium textures observed in the garnet-bearing granulite xenoliths (Bradley and
474 McCallum 1984; Farmer et al. 2005) document the growth of garnet at the expense of
475 plagioclase and orthopyroxene, and not amphibole. Furthermore, the presence or absence of

garnet in the State Line mafic lower crustal xenoliths has been interpreted to be a magmatic feature related to crystallization of basaltic melts at varying crustal depths (Bradley and McCallum 1984; Bradley 1985). Chin et al. (2020) suggested that the garnet-bearing mafic lower crust in northern Colorado represent cumulates that fractionated from primitive hydrous melts during the Proterozoic. Hence, the higher T recorded in shallower rocks garnet-absent mafic granulite xenoliths could be due to a different UHT metamorphism event that did not affect the lowermost, garnet-bearing mafic lower crust. These observations have important implications for origin of F-rich amphibole, and the apparent UHT conditions of their formation.

Origin of F-rich amphibole and ultrahigh temperature metamorphism

The F- and Cl-rich composition of the State Line amphiboles could originate from halogen enrichment processes, such as: 1) concentration of halogens in residuum following partial melting, 2) a F- and Cl-rich protolith, and/or 3) an external addition of F- and Cl-rich fluid. Partial melting experiments demonstrate that F abundance in phlogopite will increase when it is in equilibrium with a melt phase (Dooley and Patiño Douce 1996). This predicts that as the modal abundance of hydrous phases decreases during melting, residual phases will become enriched in F. In the case of the State Line xenoliths, this model predicts that the modal abundance of amphibole would decrease with partial melting, and that the remaining amphibole would re-equilibrate to greater F abundances. However, such a trend is not apparent in the State Line xenoliths; the sample with the highest modal abundance of amphibole (20 modal %) has F-rich amphibole that contains approximately 1 wt.% F (Fig. S3). Furthermore, Cl has a slightly larger ionic radius than F and should behave more incompatibly during partial melting, creating a negative relationship between F and Cl concentrations; in contrast, our data show a clear positive

trend (Fig. 2b). We conclude that a halogen-enriched residuum is the least likely explanation for the origin of F-rich amphibole in the State Line xenoliths.

The State Line xenoliths are interpreted to have been Paleoproterozoic arc-derived basaltic melts that intruded into the deep crust and underwent fractional crystallization (Bradley and McCallum 1984; Farmer et al. 2005; Chin et al. 2020) and therefore could have retained their igneous compositions. However, experiments run at deep crustal *P-T* conditions yield amphibole-melt partition coefficients that would require the State Line amphiboles to have equilibrated with a melt with >1.1 wt% Cl (Hauri et al. 2006; Dalou et al. 2012). The high F and Cl contents could be related to some combination of fractional crystallization or inheritance from the melt source. Arc-related basalts with relatively high F (>500 ppm) and Cl (1000 to 10000 ppm) abundances in olivine-hosted melt inclusions have been observed, and numerical modeling indicates the highest halogen abundances are derived from partial melting of eclogitic facies of altered ocean crust in the subducting slab (Van den Bleeken and Koga 2015). Therefore, the most likely scenario for generating arc basalts with >1 wt% Cl involves slab melts derived from a mixture of altered oceanic crust and metasedimentary sources (Van den Bleeken and Koga 2015). Farmer et al. (2005) noted the presence of inherited Archean (3.2 Ga) zircon in the State Line lower crust xenoliths, and they could be evidence for sediment derived from Archean craton during the Paleoproterozoic assembly of continental crust in Colorado, but more work is needed to test this interpretation.

An alternative explanation for the presence of F-rich amphibole that equilibrated at UHT grades is that the amphibole in the State Line xenoliths formed by interaction with an externally derived fluid. Hot, F-rich fluids are hypothesized to be the source for F-rich pargasite in mafic granulites in east Antarctica (Tsunogae et al. 2003). Amphibole from the State Line xenoliths

have lower F/Cl ratios, as well as higher Cl and $Fe^{2+}/(Fe^{2+} + Mg)$ ratios, than those described by Tsunogae et al. (2003). These observations suggest that hot, externally derived fluids with high abundances of Fe, F, and Cl could have equilibrated with the State Line xenoliths. The source of the fluids is unclear, but they may have been exsolved from deeper crystallizing mafic magmas during prolonged episodic intrusion of mafic magma into the lower crust in the Paleoproterozoic (1.8 to 1.6 Ga), or during a later mafic underplating or intraplating event (e.g., 1.4 Ga; Farmer et al. 2005; Keller et al. 2005; Jones et al. 2010). Deep mafic intraplating and fluid exsolution might also explain why the xenolith sample SD2-LC78 has lower halogen concentrations and *T* estimates, because this xenolith originated from a shallower portion of the crust than the other samples (Fig. 3), and potentially away from hot, F rich fluids that could have equilibrated with deeper xenoliths. Likewise, intraplating mafic magmas may have pooled near the transition from the garnet-bearing lowermost crust to the structurally higher garnet-absent mafic lower crust due to the density contrast between the two rheologies. This model could explain why UHT metamorphism is not observed in the xenolith samples from the lowermost crust (Farmer et al. 2005). However, more detailed work is required to fully explore if external fluids are a viable origin for the fluorian pargasite from the State Line xenoliths.

Estimation of F and Cl abundances in garnet-free mafic lower crust.

By combining our amphibole EMPA data with modal abundance data for the same xenolith samples, we can derive a first-order estimate for F and Cl abundances in the mafic lower crust of northern Colorado. Our estimates are minima, as we do not account for halogens in nominally anhydrous minerals, nor did we analyze the trace apatite (average 2 modal %) present in the State Line mafic granulites (Bradley 1985). Assuming apatite in the xenoliths have 2 wt% F would add 0.04 wt% F to our whole-rock estimates, but because we did not analyze apatite we

use a more conservative value based only on the amphibole compositions. Using this approach, we estimate the analyzed xenoliths contain at least 0.04–0.20 wt% F and 0.02–0.10 wt% Cl. Average mafic lower crust contains 0.057 and 0.025 wt% F and Cl, respectively (Rudnick and Gao 2003). Our estimates indicate the garnet-free mafic lower crust in northern Colorado could be enriched in F and Cl by 3.5 to 4 times that of average mafic lower crust. Sample SD2-LC78, which we interpret as coming from a shallower source than the other xenoliths, yields the lowest F estimate (0.04 wt%), which is comparable to average mafic lower crust (Rudnick and Gao 2003). We tentatively interpret these data to reflect variable F and Cl abundances within the garnet-free mafic lower crust, potentially with lower values in shallower rocks.

The origin of Cretaceous to Oligocene magmas: Insights from geochemical data

The observations above demonstrate that portions of garnet-free mafic lower crust in the southern Rocky Mountains were enriched in F and Cl relative to average crustal abundances, that this enrichment occurred before the xenoliths were entrained in Devonian kimberlites, and that the deep crust in the region may have undergone high- to ultrahigh temperature granulite metamorphism. Seismic refraction studies suggest that mafic metamorphic rocks are present in the lower crust throughout the southern Rocky Mountains (e.g., Snelson et al. 2005), and therefore the mafic lower crust could be a source for silicic melts generated during Laramide compression, post-Laramide transition, and younger continental extension. In the following, we use geochemical data to revisit the discussion of silicic magma sources in the Never Summer batholith and Colorado Mineral Belt, and we put the generation of F-rich silicic magmas into a broader regional context. First, we examine biotite geochemical data from the Never Summer batholith, then we consider new trace element geochemistry, Pb, Sr, and Nd isotopic compositions, as well as previously published data, including information from Climax-type Mo

deposits (Farmer and DePaolo 1984; Stein 1985; Stein and Crock 1990) and recent Ca isotopic investigations (Mills et al. 2018).

Interpretation of Never Summer batholith biotite data.

Biotite across the Never Summer batholith have a large range of $X_{phlogopite}$, but there is little variation within individual samples (Fig. 4). There is negative correlation between Mg/(Mg + Fe_{total}) and Ti abundances that could, in part, correspond to different biotite equilibration temperatures across the batholith (Fig. 4c). Titanium in biotite temperature estimates for the Mount Richthofen pluton overlap temperature estimates calculated by Jacob et al. (2015) with the two-feldspar thermometer (Putirka 2008; approximately 730 to 780 ˚C in this study versus 700 to 780 ˚C from Jacob et al. 2015). Both log(F/OH) and log(Cl/OH) are negatively correlated with $X_{phlogopite}$ across the entire dataset (Fig. 4b,d). A negative correlation between F abundances and $X_{phlogopite}$ goes against commonly observed Mg-F association (or Fe-F avoidance) in biotite (e.g., Munoz 1984). Biotite from two Mount Cumulus samples have extremely low $X_{phlogopite}$ components and high F relative to the sample from the western portion of the pluton (Fig. 4d). The whole rock geochemistry of these two samples also yielded comparably high FeO_{tot}/(FeO_{tot} + MgO) and distinctly low abundances of Sr (Fig. 5, 6a; Jacob et al. 2015).

The Mount Cumulus granite has been interpreted as an intrusive equivalent to topaz rhyolites found throughout the western United States (Christiansen et al. 2007; Jacob et al. 2015). Biotite in the low Sr, high Fe/Mg Mount Cumulus samples are comparable to those from the Honeycomb Hills topaz rhyolite in Utah, with similar Fe/Mg, total Al, log(F/OH) and log(Cl/OH) values (Fig. 4c; Congdon and Nash 1991; Byrd and Nash 1993). Although the Honeycomb Hills biotite are depleted in Mg, they were erupted in a melt with 1–3 wt% F, which also goes against the concept of the Fe-F avoidance principle (Byrd and Nash 1993). These Fe-

590 rich biotite in Mount Cumulus pluton have relatively low Ti abundances similar to biotite from
591 the Mount Antero leucogranite, which could indicate they formed at relatively cool temperatures
592 (Fig. 4c), but their low $X_{phlogopite}$ values are below the Ti in biotite calibrations presented by
593 Henry et al. (2005). Biotite from the western Mount Cumulus sample (NS17-05) yield
594 equilibration temperatures between 639 and 653 ˚C. This range is comparable to Ti in biotite
595 temperature estimates for the Hideaway Park and Chalk Mountain topaz rhyolites (Fig. 4c), both
596 of which are located south of the Never Summer complex in the Colorado Mineral Belt and are
597 associated with the Henderson and Climax Mo deposits, respectively (Fig. 1; e.g., Mercer et al.
598 2015; Audétat 2015).

599 **Trace element signature for anatexis of garnet-absent lower crust**

600 Biotite from the Mount Cumulus pluton suggest that it formed from high silica magmas
601 comparable to those that result in topaz rhyolites or F-rich porphyry Mo deposits. This is
602 intriguing because trace element modeling of partial batch melting indicates that silicic magmas
603 in the Never Summer batholith are sourced from garnet-absent mafic lower crust (Jacob et al.
604 2015), which challenges previous suggestions that the Cenozoic F-rich melts in the study area
605 are from ancient felsic sources (Farmer and DePaolo 1984; Stein 1985; Stein and Crock 1990).
606 Hence, geochemical data from the Never Summer batholith provide insight about deep mafic
607 crustal anatexis and are a good starting point to reassess the role of the mafic lower crust in
608 generating melts to the south in the Colorado Mineral Belt.

609 The silicic melts in the Never Summer magma system have low Sr/Y (<20) and high
610 Rb/Sr, Nb, and Y (Fig. 6). The protolith for mafic granulite lower crust xenoliths is interpreted to
611 be hydrous (>1 wt% H_2O) arc-related basaltic melts (Farmer et al. 2005; Chin et al., 2020), and
612 therefore the Sr/Y ratio of silicic melts derived from deep mafic crustal anatexis is likely

613 controlled by the stability of amphibole (± garnet) in the source (Jacob et al., 2015). The low
614 Sr/Y, high Nb and Y trace element signature is also observed in F-rich leucogranites from Mount
615 Antero, as well as high silica rocks related to Mo mineralization at Climax and Henderson (Fig.
616 6). These observations indicate that amphibole in garnet-absent mafic lower crust could be
617 controlling Sr/Y values in silicic magma systems throughout the area (i.e., Never Summer
618 batholith and the Colorado Mineral Belt), and that breakdown of amphibole-bearing mafic lower
619 crust might be a critical process for generating F-rich leucogranites.

620 Previous geochemical investigations in the Colorado Mineral Belt suggested that the
621 early, F-poor Laramide suite was derived in part by mafic crustal anatexis (Stein and Crock
622 1990). This suite has notably higher Sr/Y values, and in some magma systems Sr/Y is greater
623 than 40 (e.g., Twin Lakes pluton, Breckenridge-Alma-Leadville area; Fig. 6). These samples
624 have correspondingly low Nb, Y, and Rb/Sr. We hypothesize that the high Sr/Y compositions are
625 the product of partial melts generated at deep crustal conditions (i.e., high pressure) where
626 amphibole (or garnet) are stable phases, but plagioclase was unstable. Thus, if the Laramide suite
627 involved anatexis of deep mafic crust, then we suggest the F-rich amphibole such as those we
628 observed in the State Line xenoliths remained stable.

629 The trace element data support secular changes in the style of melting from Laramide to
630 Oligocene magmatism. However, Sr/Y values can be influenced by involvement from felsic
631 material (Moyen 2009), or by differentiation of deep hydrous mafic melts beneath thick crust
632 (Chiaradia 2015; Lee and Tang 2020). That is, the secular changes in trace element abundances
633 or their ratios is also a function of the starting source composition, and previous work in the
634 Colorado Mineral Belt has argued for contributions from ancient felsic crust (Farmer and
635 DePaolo 1984; Stein and Crock 1990), or ancient metasomatized lithospheric mantle (Pettke et

636 al. 2010). Disentangling what sources may have contributed to these magmas is further
637 considered by evaluating spatial and secular patterns in Pb, Sr, and Nd isotopic data from the
638 region.

639 **Regional characteristics of Pb, Sr, and Nd isotopic data.**

640 The initial Pb isotope data from the Colorado Mineral Belt and Never Summer batholith
641 mostly plot between growth curves for average crust (Stacey and Kramers 1975) and the
642 continental lithospheric mantle (CLM) model for the western United States (Pettke et al. 2010;
643 Fig. 7). Some samples contain Pb isotope compositions that plot above growth models in
644 $^{208}Pb/^{204}Pb$ – $^{206}Pb/^{204}Pb$ space, most notably intrusions from the Henderson porphyry Mo
645 deposit (Stein 1985). The Henderson intrusions likely incorporated a small fraction (<5%) of Pb
646 from unusually Th-rich host rock with high $^{208}Pb/^{204}Pb$ (Silver Plume Granite; Stein 1985).
647 Available Pb isotopic data for other upper crustal Proterozoic rocks in the region generally have
648 variable and high $^{208}Pb/^{204}Pb_{35\ Ma}$, which plot above the CLM growth curve (Frazer 2017; Fig.
649 7d). If upper crustal contamination was significant, we would expect to see higher, and more
650 variable, $^{208}Pb/^{204}Pb_i$ values in the samples we analyzed. The Pb isotopic data therefore do not
651 support significant upper crustal contamination. Instead, most of the magmatism in the area can
652 be described either as: 1) a mixture between a low U/Th end member and another end member
653 with average crustal Pb (i.e., Stacey and Kramers two-stage Pb), or 2) a product of reservoirs
654 where Th/Pb and U/Pb were variably fractionated in the Proterozoic (approximately 1.8 to 1.7
655 Ga; Stein 1985; Pettke et al. 2010).

656 A compilation of new and existing Sr and Nd isotopic data for Cretaceous and younger
657 igneous rocks and Proterozoic country rocks indicates that ancient mafic lower crust has isotopic
658 compositions similar to many of the magma systems analyzed in this study (Fig. 11). Cretaceous

basalts from the Windy Gap formation are inferred to have been derived from enriched lithospheric mantle and also have Sr-Nd isotopic compositions that overlap with the mafic lower crust (Bailley 2010; Fig. 11). Based on these Sr-Nd isotopic data, the samples we analyzed from the Colorado Mineral Belt could have either: (1) large contributions from ancient mafic lower crust, or (2) a two-component mixture of enriched mantle and ancient felsic crust sources. However, deciphering the exact contributions of mantle and crustal sources with these data alone can be ambiguous (e.g., Pettke et al. 2010; Mills et al. 2018). For example, the Mount Princeton batholith and Mount Antero leucogranite have Nd isotopic compositions that are comparable to mafic xenoliths in the region (Fig. 11), but radiogenic Ca isotopes indicate that only the Mount Princeton batholith contains significant ancient felsic crustal material (Mills et al. 2018). The F-rich Mount Antero leucogranite has relatively unradiogenic Ca isotopes, consistent with derivation from a low K/Ca (e.g., mafic lower crust) or juvenile mantle-derived source (Mills et al., 2018). Porphyries related to Mo mineralization in the Colorado Mineral Belt have a narrow range of εNd_i (approximately -8 to -10) that overlaps the Mount Antero leucogranite (Fig. 11), which is consistent with derivation from a similar mafic crustal source. The silicic intrusions from the Never Summer complex have εNd_i values much higher than those of ancient felsic country rocks (Fig. 11), and therefore likely incorporated only minor amounts of ancient felsic crustal material (Jacob et al. 2015). The Grizzly Peak caldera complex has the lowest εNd_i values (<-12), and some of the post-caldera intrusions overlap ancient felsic country rocks (Fig. 11a). Calcium isotope data corroborate incorporation of significant ancient felsic material into the Grizzly Peak Tuff (Mills et al. 2018). The Grizzly Peak caldera therefore has the strongest evidence for incorporation of large amounts of ancient felsic crust relative to many other Laramide and younger magma systems in the central Colorado Mineral Belt.

Magma systems in the northern Colorado Mineral Belt and Never Summer mountains generally have more radiogenic Pb and less radiogenic Nd compositions than those in the central Colorado Mineral Belt (Figs. 7, 9; Stein 1985; Stein and Crock 1990). There is a lack of correlation between silica content and the isotopic composition of Nd and Pb across the entire dataset (i.e., Never Summers, northern and central Colorado Mineral Belt), so the spatial variations are not solely due to variable contributions from laterally homogenous isotopic reservoirs of ancient crust and mantle end members (Figs. 7, 9). Instead, these data support inferences for isotopically heterogeneous source material in central and northern Colorado, perhaps with varying degrees of ancient granulitization of the deep crust that variably fractionated parent-daughter elements (Stein and Crock 1990) or with multiple episodes of metasomatism of the upper mantle during (i.e., during Proterozoic subduction and again during Laramide flat slab subduction; Pettke et al. 2010; Sun et al. 2021). Each of these processes can modify the parent-daughter ratios of isotopic systems or modify the isotopic compositions without significantly changing the major element composition of the reservoir. The lateral heterogeneities observed here and elsewhere (e.g., Stein and Crock 1990) are due to variations in Rb-Sr, Sm-Nd, and U-Th-Pb isotopic systems depending on their metamorphic and metasomatic histories.

Secular variations in magmatism.

Secular variations in Pb isotopic compositions support the hypothesis that F-rich leucogranites and topaz rhyolites are derived from different sources than their precursor intrusions. For example, $^{206}Pb/^{204}Pb_i$ is observed to decrease through time in a given area, including (Fig. 12): 1) the 39.7 Ma pre-Mo white dikes from the Alma district relative to the 33 to 25 Ma intrusions from the Climax Mo mine and the 26.2 Ma Chalk Mountain rhyolite

(Bookstrom 1989; Rosera et al. 2021); 2) the Paleocene phase of the Twin Lakes pluton relative to the Eocene phase and rhyolite porphyry from the Middle Mountain porphyry Mo deposit; 3) the Mount Princeton quartz monzonites that are intruded by the Mount Antero leucogranites; and 4) early silicic dikes from the Never Summer complex contain more radiogenic Pb than the younger Mount Cumulus leucogranite. These data corroborate previous observations that young leucogranites and topaz rhyolites tend to have the least radiogenic Pb isotope compositions in any given area (Stein 1985).

The progression of magmatism from Laramide compression through extension/Rio Grande rifting can therefore be described as deriving from isotopically variable reservoirs in both space and time. Leucogranites across Colorado that are compositionally similar to each other in terms of trace elements were generated from isotopically distinct lithospheric domains, yet they follow a similar temporal-isotopic pattern relative to their precursor intrusions. For example, the Pb (and Nd) isotopic compositions of the Mount Cumulus leucogranites do not overlap with the Mount Antero leucogranites or Chalk Mountain rhyolite, but all of these high-silica rocks have slightly lower $^{206}Pb/^{204}Pb_i$ than the intrusions that precede them. A source with low time-integrated U/Pb (and U/Th) is thus the likeliest one for F-rich silicic melts, but the degree of retardation of uranogenic Pb varies regionally. It is unclear if the spatial variation was inherited from ancient crust, possibly due to variability in proposed UHT metamorphism and F-enrichment, or if the spatial variation is related to long-term modification of the lower crust by an influx of melts derived from an enriched mantle source with laterally heterogeneous Pb isotope compositions.

The Grizzly Peak caldera and the role of ancient felsic crust.

Radiogenic isotopic data, including analyses from Mo-mineralizing intrusions in the Colorado Mineral Belt, have been used to argue that melting of ancient felsic crust is essential for generating the F-rich high silica magmas that formed topaz rhyolites and porphyry Mo systems (Farmer and DePaolo 1984; Stein and Crock 1990), but data presented here and elsewhere (Mills et al. 2018) suggest magmas with the clearest evidence for significant contributions from felsic crust are not necessarily F-rich rocks. For example, the ~34.3 Ma Grizzly Peak Tuff (McIntosh and Chapin 2004) and resurgent plutons in its caldera have Nd isotopic compositions that overlap with felsic country rocks (Fig. 11), and a significant component of felsic Proterozoic crust in the tuff is supported by excess ^{40}Ca (Mills et al. 2018). Fridrich et al. (1991, 1998) observed discontinuous rings of hydrothermally altered dikes and stocks outside of the Grizzly Peak caldera, some of which have been prospected for porphyry Mo, but our new data suggest these intrusions are not directly related to the Grizzly Peak system. A 34.0 Ma hydrothermally altered dike east of the caldera yields εNd_i = -8.7, whereas the Grizzly Peak tuff and intrusions have $\varepsilon Nd_i \approx$ -12.5 (Table S6; Figs. 9, 11; Johnson and Fridrich 1990). Likewise, the 36.45 Ma low-grade Mo-F porphyry system at Middle Mountain, southeast of the caldera, predates the eruption of the tuff (Rosera et al. 2021), and the Middle Mountain porphyry has more radiogenic Nd than the Grizzly Peak system (Fig. 11b). Therefore, the Grizzly Peak caldera contains the rocks in the Colorado Mineral Belt with the lowest εNd_i and perhaps the greatest contribution of ancient felsic sources, but the caldera rocks do not appear to be similar to topaz rhyolites, nor has deep exploration identified any significant Mo mineralizing intrusions related to the caldera-forming magma system. It is possible that such a system could occur at depth, perhaps below volcanic cover within the caldera, but there is currently no

749 evidence that the ancient felsic crustal-derived Grizzly Peak magmas generated any topaz
750 rhyolites or Mo mineralization.

751 **Tracing F and Cl from mafic lower crustal anatexis to upper crustal silicic magma systems**

752 The biotite data presented in this study corroborate interpretations that the Mount
753 Cumulus pluton is an intrusive analogue to topaz rhyolites (e.g., Jacob et al. 2015), including
754 those erupted from the Climax-type deposits in the Colorado Mineral Belt. Melt inclusions and
755 analysis of volcanic glass indicate that topaz rhyolites typically have >2000 ppm F and F/Cl > 3
756 (Christiansen et al., 2007; Audétat 2015; Mercer et al. 2015), but reliable F and Cl estimates for
757 their intrusive equivalents are scarce because whole-rock data cannot account for volatile loss. In
758 the following section, we use recently calibrated biotite-melt exchange equations to estimate
759 melt abundances of F and Cl in the Never Summer batholith, and we compare those data to batch
760 melting models derived from analyses of garnet-free mafic lower crustal xenoliths. These models
761 require various assumptions about: (1) how F/OH and Cl/OH partition between biotite and silicic
762 melt, (2) the saturation concentration and speciation of water in melts based on whole rock data,
763 (3) the behavior of volatiles (i.e., F and Cl) during open-system crystallization, and (4) the
764 degree of post-solidification re-equilibration. We emphasize that these models are first-order
765 approximations of the magmatic compositions of F and Cl in silicic intrusions, but by
766 approaching the question from the source (i.e., xenolith data) to the sink (i.e., Never Summer
767 batholith), we hope to gain further perspective about how deep crustal anatexis might lead to
768 assembly of F-rich magma systems. To better validate these models, we compare our estimated F
769 and Cl abundances in the Never Summer batholith to melt inclusion data from the Colorado
770 Mineral Belt, as well as F and Cl estimates from average whole-rock and biotite data from the
771 Mount Princeton batholith and Mount Antero leucogranites (Toulmin and Hammarstrom 1990).

This is the peer-reviewed, final accepted version for American Mineralogist, published by the Mineralogical Society of America.
The published version is subject to change. Cite as Authors (Year) Title. American Mineralogist, in press.
DOI: https://doi.org/10.2138/am-2022-8503. http://www.minsocam.org/

Estimating F and Cl in silicic melt from biotite and whole rock data.

Melt F and Cl abundances were estimated following the recent formulations of Zhang et al. (2022). Their models calculate biotite-melt partition coefficients for F/OH and Cl/OH ($Kd_{F/OH}^{biotite\text{-}melt}$ and $Kd_{Cl/OH}^{biotite\text{-}melt}$, respectively; Table S2). The exchange partition coefficients for each are function of $X_{phlogopite}$ (which they refer to as X_{Mg}) and Ti in biotite and melt F or Cl can be calculated by assuming water saturation and speciation models. Zhang et al. (2022) use the whole rock major element data and formulations of Moore et al. (1998) to model H_2O_{melt}, and the Behrens (2020) water speciation model. Modeled H_2O_{melt} values are sensitive to estimated pressure, and to a lesser degree, temperature. Aluminum in amphibole geobarometry from the Mount Richthofen pluton yielded an average pressure estimate of 100 MPa (Jacob et al. 2015), which overlaps pressure estimates derived from melt inclusion data for the Hideaway Park topaz rhyolite in the Colorado Mineral Belt (approximately 60 to 70 MPa; Mercer et al. 2015). We calculated H_2O_{melt} abundances at 50 and 100 MPa with an input temperature of 750 ˚C. These estimates yield a range from approximately 3 to 4.5 wt% H_2O_{melt} at 50 and 100 MPa, respectively. The calculated H_2O_{melt} abundances for the Never Summer batholith overlap those reported from quartz-hosted melt inclusions from the Hideaway Park and Chalk Mountain topaz rhyolites in the Colorado Mineral Belt (approximately 2 to 5 wt% H_2O; Audétat 2015; Mercer et al. 2015). Using these data, we estimated F and Cl in melt using biotite and whole rock data from the Never Summer batholith as well as Mount Princeton batholith and Mount Antero leucogranite (Toulmin and Hammarstrom 1990; Table 2). Estimated F melt concentrations in equilibrium with biotite from the Mount Cumulus pluton at 50 MPa have a large range, from 0.88 to 6.8 wt%. At 100 MPa, the F concentrations reach 9 wt%. It is possible that these unusually high estimates are affected by re-equilibration with late-stage, F-rich fluids after

crystallization, but whole-rock geochemical data still support that these samples are more evolved in terms of their trace element abundances (Fig. 6). Estimated Cl abundances in the Mount Cumulus pluton are much lower than F in the same samples (0.11 to 0.45 wt% Cl). The Mount Richthofen pluton has lower estimated F (0.1 to 0.55 wt%) and higher Cl (0.54 to 3.2 wt%) than the Mount Cumulus pluton.

Comparison to garnet-free mafic lower crust batch melting models.

We compare the estimated F and Cl melt abundances to partial batch melting models using data from garnet-free mafic lower crustal xenoliths (Fig. 13). The partial melting models were constructed using the minimum F and Cl whole rock concentrations discussed above (gray stars, Fig. 13) and they indicate that 1 to 5% melting would yield a melt with approximately 1000 to 5000 ppm F, and 2000 to over 10000 ppm Cl. Batch melting models for the xenoliths richest in F and Cl are in good agreement with estimated F and Cl melt abundances for the silicic member of the Mount Richthofen pluton (purple triangles; Fig. 13). This observation corroborates previous batch melting models with Sr/Y and La/Yb that suggested that the silicic member of the Mount Richthofen pluton is a reasonable analogue to low-degree partial melts from garnet-free mafic lower crust (Jacob et al. 2015). These data, along with trace element and isotopic data presented in this study (Fig. 11) and Jacob et al. (2015), demonstrate that F-rich (i.e., >2000 ppm F) silicic melts in the Never Summer batholith formed from mafic lower crustal anatexis.

Estimated melt F and Cl abundances for the mafic member of the Mount Richthofen granodiorite and all three samples from the Mount Cumulus pluton are not near any of the partial melting models we generated (Fig. 13). The Mount Cumulus samples have higher F abundances that what is predicted for partial melts based on the xenolith data, but their deviation could be

explained by fractionation of F/Cl during crystallization with open-system degassing. The blue arrows in Figure 13 show H_2O-saturated crystallization models after Candela (1986) for magmas at 4.5 and 3 wt% H_2O; the black arrow shows how F and Cl increase with H_2O-undersaturated crystallization. Chlorine is preferentially partitioned into the fluid phase relative to the melt during degassing, but it also behaves incompatibly during crystallization. Fluorine also behaves incompatibly during crystallization but tends to stay in the melt phase during open-system degassing. As such, H_2O-saturated crystallization of melts with more than ~2.5 wt% H_2O have a negative slope on Figure 13 (e.g., more Cl in the melt is lost to the fluid phase than what is gained from crystallization; Candela 1986). Finally, the H_2O concentration at saturation might not be constant, because F, an incompatible element during crystallization, increases H_2O saturation in melt (Holtz et al. 1993). Hence, H_2O-saturated crystallization may not necessarily follow a linear path on Figure 13.

The models presented in Figure 13 suggest that low-degree partial melts from the F-rich mafic lower crust, such as the silicic member of the Mount Richthofen pluton, could represent primitive melts that, upon crystallization and open-system degassing, become enriched in F and F/Cl. This corroborates conclusions from Jacob et al. (2015) that the Mount Cumulus leucogranite formed from melts that formed following differentiation of primitive silicic melts comparable to the silicic member of the Mount Richthofen pluton, but high-precision geochronological data preclude that the two plutons are directly related (Jacob et al. 2015; Rosera et al. 2021).

Fluid-saturated fractional crystallization modelling of primitive low silica rhyolite melts has been used to explain trace element variations and F enrichment in the Chalk Mountain and Hideaway Park topaz rhyolites from the Colorado Mineral Belt (Audétat 2015; Mercer et al.

2015). Low-degree batch melting models for F-rich garnet-free mafic lower crust, accompanied by H_2O-saturated fractional crystallization, could also explain the F and Cl abundance measured in melt inclusions from these two topaz rhyolites (Fig. 13), thereby supporting a mafic crustal source for primary F enrichment in their primitive silicic melts. Estimated F abundances for averaged data from the Mount Antero leucogranite are lower than estimates from Mount Cumulus and measurements from melt inclusions from the Chalk Mountain and Hideaway Park rhyolites (Fig. 13). It is unclear if these differences are related to different source material (i.e., lower F) or the degree of shallow crustal differentiation, but these data do suggest that the silicic melts that formed the Mount Antero leucogranite also had >2000 ppm F, similar to the silicic member of the Mount Richthofen pluton.

Estimated F and Cl abundances for the Mount Princeton batholith indicate it had a much lower F/Cl than other systems we considered. Likewise, quartz-hosted melt inclusions from the Alma rhyolite dikes do not follow the partial melting and crystallization models. We suggest that the Mount Princeton batholith and Alma rhyolites likely come from a source with significantly different F and Cl abundances than those in the mafic lower crustal xenoliths studied here. This observation is also supported by isotopic data; both the Alma rhyolites analyzed in this study and the Mount Princeton batholith contain more less radiogenic Nd, and more radiogenic Pb than younger F-rich magmas that intruded near them (Figs. 11,12). Furthermore, Ca isotope data indicate that the Mount Princeton batholith contained significant ancient felsic crust (Mills et al. 2018), which further demonstrates that ancient felsic crust is not necessarily F-rich within the central Colorado Mineral Belt.

The mafic member of the Mount Richthofen pluton yielded the highest estimated Cl and lowest F abundances from the Never Summer batholith (Fig. 13). Jacob et al. (2015) suggested

that mantle-derived melts mixed with silicic melts derived by mafic crustal anatexis to form the Mount Richthofen pluton, and therefore it is not surprising that the mafic member of Mount Richthofen does not follow the lower crustal partial melting models shown in Figure 13. However, the estimated Cl contents range from 2 to 3 wt% for the 50 and 100 MPa models, respectively (Table S2; Fig. 13), which is greater than what has been reported for magmas with similar silica and total alkali contents (<1 wt% Cl; Webster et al. 2018). This suggests that either the mantle-derived melts in the Never Summer batholith could have been highly enriched in Cl, or that the biotite reequilibrated with Cl-rich fluids after crystallization. Evidence supporting subsolidus reequilibration for this sample include: (1) calcium amphibole compositions range from actinolite to magnesio-hornblende (Jacob et al., 2015, classified after Hawthorn et al. 2012); (2) plagioclase-amphibole thermometry from the same sample yielded subsolidus temperatures, as low as 650 ˚C (Jacob et al. 2015); (3) Ti in biotite thermometry for this sample yields lower temperatures than the silicic member of Mount Richthofen (Fig. 4c); and (4) the F and Cl melt estimates for the Mount Cumulus pluton require loss of Cl during open-system degassing (Fig. 11), and the mafic sample we used is located near the contact with Mount Cumulus (Fig. 1). Given these observations, we tentatively suggest that amphibole and biotite in the mafic Mount Richthofen sample used in this study and by Jacob et al. (2015) are affected by post-crystallization reequilibration. More data from mafic, mantle-derived igneous rocks in the region are required to further test if they are unusually enriched in Cl.

Integrated evidence for a F-rich mafic lower crust source

Integrating data from a variety of sources leads us to conclude that F-enrichment of mafic lower crust was an essential process before later anatexis and generation of F-rich magmas in the southern Rocky Mountains. Although enriched lithospheric mantle and mafic lower crust overlap

887 in their inferred Sr, Nd, and Pb isotopic compositions (e.g., Fig. 11), other lines of evidence
888 preclude an exclusively juvenile mantle-derived source. Climax-type prospects in the Sawatch
889 Range, as well as older, F-poor Laramide intrusions, contain numerous xenocrystic zircon with
890 $^{207}Pb/^{206}Pb$ ages between 1.7 and 1.4 Ga (Feldman 2010; Rosera et al. 2021), consistent with
891 zircon ages from mafic granulite xenoliths (Farmer et al. 2005). These data indicate that at least
892 the early low-grade Mo prospects interacted with ancient crustal material and cannot solely be
893 the product of juvenile mantle-derived melts.

894 We suggest that Oligocene F-rich melts in the study area were predominately sourced
895 from ancient mafic crust, but there is enough ambiguity in the isotopic composition of the
896 mantle-derived end member that calculating specific proportions is challenging. The bimodal
897 Never Summer batholith is perhaps best suited to unraveling relationships between mantle-
898 derived melts and anatexis of mafic crust (Jacob et al. 2015). Trace element abundances
899 estimated from batch melting models presented here (Fig. 13) and elsewhere (Sr/Y and La/Yb;
900 Jacob et al. 2015) as well as radiogenic isotopic data suggest that silicic melts involved in
901 assembling the Never Summer batholith were derived from anatexis of garnet-free mafic lower
902 crust. Importantly, these silicic melts may have been enriched in F (2000 to 3000 ppm) from
903 their ancient crustal source (Fig. 13), and the elevated F/Cl ratios can be explained by H_2O-
904 saturated crystallization of these primitive melts to high-silica granites and rhyolites. Thus,
905 genetic models for topaz rhyolites and F-rich leucogranites do not necessarily require that the
906 elevated F/Cl ratios are inherited from melting juvenile, mantle-derived lower crust (e.g.,
907 Christiansen et al. 2007), but that is not to say that mantle-derived melts do not play any role in
908 generating the F-rich high silica magmas.

909

Ultimately, these observations suggest that (1) ancient felsic crust is not a critical component for generating F-rich rhyolite and leucogranites, (2) a solely juvenile, mantle-derived origin for these F-rich systems is also unlikely, and that (3) a combination of ancient, F-rich mafic lower crust ± juvenile mantle-derived melts that supply heat (and potentially some material), such as in a deep crustal hot zone (Annen et al. 2006) or hybridized zone (Rosera et al. 2013; Dailey et al. 2018), is most compatible with data presented here and elsewhere.

IMPLICATIONS

Crustal Pre-Enrichment Leading up to Fluorine-Rich Silicic Magmatism

High-F rocks have been hypothesized as a viable source for F-rich silicic magmas (e.g., Audétat 2015), and our data allow us to narrow down where, when, and how much F enrichment occurred in the magma source. Parts of the garnet-absent mafic lower crust in northern Colorado contain up to 20 modal percent F-rich amphibole, resulting in whole-rock F concentrations at least 3.5 times greater than average mafic crust (Rudnick and Gao 2003). Trace element modeling using xenolith amphibole compositions reproduces estimated F contents for inferred primitive silicic melts in the Never Summer batholith (Fig. 13), and isotopic and geochemical data support a mafic lower crust source for those rocks (Fig. 11; Jacob et al. 2015). Fluorine enrichment must have occurred prior to Laramide hydration due to the age of the xenoliths (e.g., Humphreys et al. 2003), and it could be an ancient feature of the mafic lower crust that extends throughout the southern Rocky Mountain region (Snelson et al. 2005). Our results suggest that ancient enrichment of F in the deep mafic lower crust, either by UHT granulite grade metamorphism or deep crustal magma processes (e.g., Chin et al. 2020), could be a necessary pre-condition for generating F-rich silicic magmas at a later stage.

In light of xenolith compositions reported here, we suggest that F-rich leucogranites and rhyolites in the Colorado Mineral Belt and Never Summer complex inherited their initially high halogen abundances mainly from their lower crustal source. Amphiboles are the dominant hydrous phase in the garnet-free mafic granulite xenoliths of the State Line district (Bradley 1985) and their breakdown ultimately drives variations in primary melt F and Cl concentrations. Experimental data and thermodynamic modeling demonstrate increasing the X_F of pargasite above approximately 0.4 corresponds to a thermal stability increase of 100–150 °C over F-poor pargasite (Holloway and Ford 1975; Tsunogae et al. 2003). We hypothesize that intrusion of hot, mantle-derived melts during extension heated the lower crust and induced anatexis.

This hypothesis has significant implications for models of the origin of F-rich porphyries and topaz rhyolites in the Colorado Mineral Belt and western North America. Laramide magmas have isotopic compositions consistent with derivation from mafic lower crust ± mantle, as well as slightly elevated Sr/Y and low F contents that could represent melts formed below the stability limit of F-rich amphibole. Spatio-temporal analyses indicate F-rich silicic magmatism in the southern Rocky Mountains began within a million years of the start of a regional ignimbrite "flare-up" (Rosera et al. 2021), and major Mo deposits at Henderson, Climax, Mount Emmons, and Questa all formed during later rifting events (e.g., Carten et al. 1993). Thus, the deposits formed during periods of increased invasion of mantle-derived melts into the crust, which significantly elevated the temperature of the mafic lower crust (e.g., Farmer et al. 2008) and led to the breakdown of F-rich amphibole (Fig. 14). The high heat flow during the flare-up and initial rifting therefore represents a distinctly different style of melting than during the Laramide (e.g., before the ca. 38 Ma ignimbrite flare-up).

This interpretation does not necessarily require that F-rich leucogranites are sourced from shallower crust than their precursors (e.g., Stein and Crock 1990), and we suggest that shallower crust is not likely to have been a major source for F-rich magmas. The xenolith we analyzed with the lowest estimated equilibrium P (sample SD2-LC78; approximately 0.5 GPa) also contains trace biotite and has the lowest F contents in amphibole; therefore, shallower mafic crust may not have been F-rich. In addition, seismic refraction data indicate crust in Colorado shallower than 20–25 km is more likely to be felsic (Snelson et al. 2005). The fact that magmatic systems in the Colorado Mineral Belt strongly linked to deep melting of ancient felsic crust (Grizzly Peak and Mount Princeton; Mills et al. 2018) lack significant F-rich alteration and porphyry Mo mineralization further rules out the need to infer changing sources due to a shallower magma source. Instead, we suggest that the F/OH ratio of the mafic crust could be heterogenous vertically and laterally, with high F/OH rocks restricted to the deeper crust. Thus, high F/OH rocks only melt during periods of high heat flow or direct interaction with mantle-derived melts. In this model, rocks with average-to-low F/OH are likely to melt earlier.

Implications for porphyry Mo mineralization

In a recent synthesis of isotopic data for Mesozoic porphyry Mo deposits in China, Shu and Chiaradia (2021) suggested that the magma source rocks are not pre-enriched in Mo prior to mineralization, and that there is significant isotopic diversity across different systems where deposits can incorporate juvenile or ancient lower crust with varying proportions of mantle-derived melt. Our study suggests that pre-enrichment of F, rather than Mo, could be a critical prerequisite for the genesis of large porphyry Mo deposits, and that in the case of the southern Rocky Mountains it is the ancient mafic lower crust that hosts F-rich rocks. Consequently, the isotopic diversity of porphyry Mo deposits noted by Shu and Chiaradia (2021) could reflect

977 varying degrees of F enrichment throughout heterogeneous lithosphere. Fluorine-rich silicic
978 melts derived from these enriched sources will have higher H_2O saturation (Holtz et al. 1993), as
979 well as lower viscosity and solidi than their low-F counterparts (Manning 1981; Ouyang et al.
980 2020). Consequently, melts with high initial F upon ascent into the upper crust can achieve high
981 levels of magmatic differentiation and expel large volumes of water, both processes that favor
982 the development of porphyry Mo systems with high F/Cl ratios (e.g., Audétat 2015).

983 Our results provide information regarding how much F-enrichment is needed to set the
984 stage for generating silicic magmas capable of forming a porphyry Mo deposit. Batch melt
985 modeling demonstrates that parts of the garnet-absent mafic lower crust in northern Colorado can
986 generate primary silicic melts with >2000 ppm F (Fig. 13). Estimated F abundances from biotite-
987 silicic melt formulations demonstrate that primitive silicic melts in the Never Summer batholith
988 also contained >2000 ppm F, and fluid-saturated crystallization in the shallow crust can drive F
989 contents to 1 to 5 wt% F (Fig. 13). The similarity of F and Cl estimates for the Mount Cumulus
990 leucogranite to melt inclusions measurements for topaz rhyolites related to porphyry Mo
991 mineralization in the Colorado Mineral Belt implies the silicic magmas that formed the Mount
992 Cumulus pluton are comparable to mineralizing intrusions in porphyry Mo deposits. Importantly,
993 they attained these extreme levels of fractionation because they formed from low-degree partial
994 melts that had >2000 ppm F (and correspondingly a suppressed solidus and decreased viscosity)
995 upon ascent into the shallow crust. It is possible to generate high F and F/Cl from primitive melts
996 with low F (e.g., <1000 ppm) abundances through extensive (>80%) H_2O-saturated fractional
997 crystallization (blue arrows; Fig. 13), but this pathway to F enrichment is less probable because
998 the higher melt viscosity relative a F-rich starting melt would inhibit crystal-liquid separation,
999 and the higher solidus temperature leads to earlier rheological lock up. Thus, pre-enrichment of

deep crustal sources in F might not be a requirement for generating F-rich granites and rhyolites, but higher initial F abundances make extreme levels of differentiation more likely, and in turn could explain why the largest known Climax-type deposits are highly concentrated in Colorado (Ludington and Plumlee 2009).

High-precision U/Pb zircon geochronology on the same samples we used in this study indicate the Mount Cumulus pluton was assembled over 10's to 100's of k.y. (Rosera et al. 2021). Hence, silicic melts with >2000 ppm F and F/Cl near unity can differentiate rapidly; over shorter time frames than the full lifespan of porphyry Mo systems (100's to 1000's of k.y.; Gaynor et al. 2019; Zhao et al. 2021). Existing models have hypothesized that S in porphyry Mo is introduced by small volumes of mafic melts, rather than being from the causative silicic magmas (Mercer et al. 2015). The evidence for rapid differentiation, and therefore rapid fluctuations in F (and Cl), coupled with the required external introduction of S could explain the paucity of F-rich porphyry Mo deposits in the geological record (e.g., Ludington and Plumlee 2009; Audétat and Li 2017), and we suggest it may have contributed to the lack of significant mineralization in the Never Summer batholith. Furthermore, the textural complexity of major mineralizing intrusions at the Henderson deposit are hypothesized to be linked to solidus depression due to high concentrations of F, whereas less texturally complex intrusions are associated with lower ore grades (Carten et al. 1988). Thus, rapid increase in F concentration and F/Cl values can explain observations where texturally complex mineralizing intrusions are punctuated by unmineralized, or low-grade intrusions, during assembly of Climax-type systems (Carten et al. 1988; Gaynor et al. 2019).

ACKNOWLEDGMENTS

This project was funded by the Martin Fund and Dissertation Completion Fellowship at the University of North Carolina at Chapel Hill. Further support was provided by the Geological Society of America and Sigma Xi. Special thanks to Aaron Bell for his help and advice with the electron microprobe and data analysis, as well as Kelsey Woody and Rebecca Finchman for helping in the field. We thank Amy Gilmer, Paul Giesting, and an anonymous reviewer for their thorough review that helped to greatly improve the manuscript. Any use of trade, firm, or product names is for descriptive purposes only and does not imply endorsement by the U.S. Government.

REFERENCES

Abbey, A.L., and Niemi, N.A. (2020) Perspectives on continental rifting processes from spatiotemporal patterns of faulting and magmatism in the Rio Grande Rift, USA. Tectonics, 39, e2019TC005635.

Annen, C., Blundy, J.D., and Sparks, R.S.J. (2006) The genesis of intermediate and silicic magmas in deep crustal hot zones. Journal of Petrology, 47, 505–539.

Aranovich, L., and Safonov, O. (2018) Halogens in high-grade metamorphism. In D.E. Harlov and L. Aranovich, Eds., The Role of Halogens in Terrestrial and Extraterrestrial Geochemical Processes: Surface, Crust, and Mantle pp. 713–757. Springer International Publishing, Cham, Switzerland.

Audétat, A. (2015) Compositional evolution and formation conditions of magmas and fluids related to porphyry Mo mineralization at Climax, Colorado. Journal of Petrology, 56, 1519–1546.

1043 Audétat, A., and Li, W. (2017) The genesis of Climax-type porphyry Mo deposits: Insights from
1044 fluid inclusions and melt inclusions. Ore Geology Reviews, 88, 436–460.

1045 Bailley, T.L. (2010) A reevaluation of the origin of late Cretaceous and younger magmatism in
1046 the southern Rocky Mountain region using space-time-composition patterns in volcanic
1047 rocks and geochemical studies of mantle xenoliths, 153 p. Ph.D thesis, University of
1048 Colorado, Boulder, CO.

1049 Behrens, H. (2020) Water speciation in oxide glasses and melts. Chemical Geology, 558,
1050 119850.

1051 Bookstrom, A.A. (1989) The Climax-Alma granite batholith of Oligocene age and the porphyry
1052 molybdenum deposits of Climax, Colorado, U.S.A. Engineering Geology, 27, 543–568.

1053 ——— (1990) Igneous rocks and carbonate-hosted ore deposits of the central Colorado Mineral
1054 Belt. Economic Geology Monograph, 7, 45–65.

1055 Bookstrom, A.A., Naeser, C.W., and Shannon, J.R. (1987) Isotopic age determinations, unaltered
1056 and hydrothermally altered igneous rocks, north-central Colorado mineral belt.
1057 Isochron/West, 13–20.

1058 Bradley, S.D. (1985) Granulite facies and related xenoliths from Colorado-Wyoming kimberlite,
1059 179 p. MSc Thesis, Colorado State University.

1060 Bradley, S.D., and McCallum, M.E. (1984) Granulite facies and related xenoliths from
1061 Colorado-Wyoming Kimberlite. In J. Kornprobst, Ed., Developments in Petrology, 11,
1062 pp. 205–217. Elsevier.

1063 Burt, D.M., Sheridan, M.F., Bikun, J.V., and Christiansen, E.H. (1982) Topaz rhyolites;
1064 distribution, origin, and significance for exploration. Economic Geology, 77, 1818-1836.

1065 Byrd, B.J., and Nash, W.P. (1993) Eruption of rhyolite at the Honeycomb Hills, Utah: Cyclical
1066 tapping of a zoned silicic magma reservoir. Journal of Geophysical Research: Solid
1067 Earth, 98, 14075–14090.

1068 Candela, P. (1986) Toward a thermodynamic model for the halogens in magmatic systems: an
1069 application to melt-vapor-apatite equilibria. Chemical Geology, 57, 289–301.

1070 Carten, R.B., Geraghty, E.P., Walker, B.M., and Shannon, J.R. (1988) Cyclic development of
1071 igneous features and their relationship to high-temperature hydrothermal features in the
1072 Henderson porphyry molybdenum deposit, Colorado. Economic Geology, 83, 266-296.

1073 Carten, R.B., White, W.H., and Stein, H.J. (1993) High-grade granite-related molybdenum
1074 systems: Classification and origin. In Mineral Deposit Modelling Vol. 40, pp. 521–554.
1075 Geological Association of Canada, Special Paper.

1076 Chapin, C.E. (2012) Origin of the Colorado Mineral Belt. Geosphere, 8, 28-43.

1077 Chiaradia, M. (2015) Crustal thickness control on Sr/Y signatures of recent arc magmas: An
1078 Earth scale perspective. Scientific Reports, 5, 8115.

1079 Chin, E.J., Curran, S.T., and Farmer, G.L. (2020) Squeezing water from a stone: H_2O in
1080 nominally anhydrous minerals from granulite xenoliths and deep, hydrous fractional
1081 crystallization. Journal of Geophysical Research: Solid Earth, 125, e2020JB020416.

1082 Christiansen, E.H., Burt, D.M., Sheridan, M.F., and Wilson, R.T. (1983) The petrogenesis of
1083 topaz rhyolites from the western United States. Contributions to Mineralogy and
1084 Petrology, 83, 16–30.

1085 Christiansen, E.H., Haapala, I., and Hart, G.L. (2007) Are Cenozoic topaz rhyolites the erupted
1086 equivalents of Proterozoic rapakivi granites? Examples from the western United States
1087 and Finland. IGCP project 510: A-type granites and related rocks through time, 97, 219–
1088 246.

1089 Clemens, J.D., Holloway, J.R., and White, A.J.R. (1986) Origin of an A-type granite;
1090 experimental constraints. American Mineralogist, 71, 317–324.

1091 Coleman, D.S., Frost, T.P., and Glazner, A.F. (1992) Evidence from the Lamarck Granodiorite
1092 for rapid late Cretaceous crust formation in California. Science, 258, 1924–1926.

1093 Congdon, R.D., and Nash, W.P. (1991) Eruptive pegmatite magma: rhyolite of the Honeycomb
1094 Hills, Utah. American Mineralogist, 76, 1261–1278.

1095 Dailey, S.R., Christiansen, E.H., Dorais, M.J., Kowallis, B.J., Fernandez, D.P., and Johnson,
1096 D.M. (2018) Origin of the fluorine- and beryllium-rich rhyolites of the Spor Mountain
1097 Formation, Western Utah. American Mineralogist, 103, 1228–1252.

1098 Dalou, C., Koga, K.T., Shimizu, N., Boulon, J., and Devidal, J. (2012) Experimental
1099 determination of F and Cl partitioning between lherzolite and basaltic melt. Contributions
1100 to Mineralogy and Petrology, 163, 591–609.

1101 Dooley, D.F., and Patiño Douce, A.E. (1996) Fluid-absent melting of F-rich
1102 phlogopite+rutile+quartz. American Mineralogist, 81, 202–212.

1103 Dostal, J., van Hengstum, T.R., Shellnutt, J.G., and Hanley, J.J. (2016) Petrogenetic evolution of
1104 Late Paleozoic rhyolites of the Harvey Group, southwestern New Brunswick (Canada)
1105 hosting uranium mineralization. Contributions to Mineralogy and Petrology, 171, 59.

1106 Dumitru, T.A., Gans, P.B., Foster, D.A., and Miller, E.L. (1991) Refrigeration of the western
1107 Cordilleran lithosphere during Laramide shallow-angle subduction. Geology, 19, 1145–
1108 1148.

1109 Emmons, S.F. (1886) Geology and mining industry of Leadville, Colorado, with atlas. U.S.
1110 Geological Survey Monograph 12, Washington, DC.

1111 Ernst, W.G., and Liu, J. (1998) Experimental phase-equilibrium study of Al- and Ti-contents of
1112 calcic amphibole in MORB; a semiquantitative thermobarometer. American
1113 Mineralogist, 83, 952–969.

1114 Erslev, E. (2005) 2D Laramide geometries and kinematics of the Rocky Mountains, western
1115 U.S.A. In K.E. Karlstrom and G.R. Keller, Eds., The Rocky Mountain Region: An
1116 Evolving Lithosphere Tectonics, Geochemistry, and Geophysics, Geophysical
1117 Monograph Series, 154, pp. 7-20. American Geophysical Union.

1118 Farmer, G.L., and DePaolo, D.J. (1984) Origin of Mesozoic and Tertiary granite in the western
1119 United States and implications for pre-Mesozoic crustal structure: 2. Nd and Sr isotopic
1120 studies of unmineralized and Cu- and Mo-mineralized granite in the Precambrian Craton.
1121 Journal of Geophysical Research: Solid Earth, 89, 10141–10160.

1122 Farmer, G.L., Bowring, S.A., Williams, M.L., Christensen, N.I., Matzel, J.P., and Stevens, L.
1123 (2005) Contrasting lower crustal evolution across an Archean: Proterozoic suture:
1124 Physical, chemical and geochronologic studies of lower crustal xenoliths in southern

Wyoming and northern Colorado. In K.E. Karlstrom and G.R. Keller, Eds., The Rocky Mountain Region: An Evolving Lithosphere Tectonics, Geochemistry, and Geophysics, Geophysical Monograph Series, 154, pp. 139–162. American Geophysical Union.

Farmer, G.L., Bailley, T., and Elkins-Tanton, L.T. (2008) Mantle source volumes and the origin of the mid-Tertiary ignimbrite flare-up in the southern Rocky Mountains, western U.S. Continental Volcanism and the Chemistry of the Earth's Interior, International Conference on Continental Volcanism, Lithos, 102, 279–294.

Farmer, G.L., Fritz, D.E., and Glazner, A.F. (2020) Identifying metasomatized continental lithospheric mantle involvement in Cenozoic magmatism from Ta/Th values, southwestern North America. Geochemistry, Geophysics, Geosystems, 21, e2019GC008499.

Feldman, J.D. (2010) The emplacement and exhumation history of the Twin Lakes batholith and implications for the Laramide orogeny and flat slab subduction, 174 p. MSc Thesis, New Mexico Institute of Mining and Technology, Socorro, NM.

Frazer, R.E. (2017) The significance of atypical high-silica igneous rocks, 167 p. Ph.D dissertation, University of North Carolina at Chapel Hill.

Fridrich, C.J., Smith, R.P., De Witt, E., and McKee, E.H. (1991) Structural, eruptive, and intrusive evolution of the Grizzly Peak caldera, Sawatch Range, Colorado. GSA Bulletin, 103, 1160–1177.

Fridrich, C.J., De Witt, E., Bryant, B., Richard, S.M., and Smith, R.P. (1998) Geologic map of the Collegiate Peaks Wilderness Area and the Grizzly Peak Caldera, Sawatch Range, central Colorado. Report.

1147 Frost, B.R., Barnes, C.G., Collins, W.J., Arculus, R.J., Ellis, D.J., and Frost, C.D. (2001) A
1148 geochemical classification for granitic rocks. Journal of Petrology, 42, 2033–2048.

1149 Frost, C.D., and Frost, B.R. (2011) On Ferroan (A-type) Granitoids: Their compositional
1150 variability and modes of origin. Journal of Petrology, 52, 39–53.

1151 Gaynor, S.P., Rosera, J.M., and Coleman, D.S. (2019) Intrusive history of the Oligocene Questa
1152 porphyry molybdenum deposit, New Mexico. Geosphere, 15, 548–575.

1153 Girei, M.B., Li, H., Vincent, V.I., Algeo, T.J., Elatikpo, S.M., Bute, S.I., Ahmed, H.A., and
1154 Amuda, A.K. (2020) Genesis and timing of Mo mineralization in the Mada Ring
1155 Complex, north-central Nigeria: insights from whole-rock geochemistry, Nd-Sr isotopes,
1156 zircon U-Pb-Hf isotopes, and molybdenite Re-Os systematics. Mineralium Deposita.

1157 Guidotti, C.V., and Dyar, M.D. (1991) Ferric iron in metamorphic biotite and its petrologic and
1158 crystallochemical implications. American Mineralogist, 76, 161–175.

1159 Hart, S. (1984) A large-scale isotope anomaly in the Southern Hemisphere mantle. Nature, 309,
1160 753–757.

1161 Harvey, J., and Baxter, E.F. (2009) An improved method for TIMS high precision neodymium
1162 isotope analysis of very small aliquots (1–10 ng). Chemical Geology, 258, 251–257.

1163 Hauri, E.H., Gaetani, G.A., and Green, T.H. (2006) Partitioning of water during melting of the
1164 Earth's upper mantle at H2O-undersaturated conditions. Earth and Planetary Science
1165 Letters, 248, 715–734.

1166 Hawthorne, F.C., Oberti, R., Harlow, G.E., Maresch, W.V., Martin, R.F., Schumacher, J.C., and
1167 Welch, M.D. (2012) Nomenclature of the amphibole supergroup. American Mineralogist,
1168 97, 2031–2048.

1169 Henry, D.J., Guidotti, C.V., and Thomson, J.A. (2005) The Ti-saturation surface for low-to-
1170 medium pressure metapelitic biotites: Implications for geothermometry and Ti-
1171 substitution mechanisms. American Mineralogist, 90, 316–328.

1172 Henry, D.J., and Daigle, N.M. (2018) Chlorine incorporation into amphibole and biotite in high-
1173 grade iron-formations: Interplay between crystallography and metamorphic fluids.
1174 American Mineralogist, 103, 55–68.

1175 Hofstra, A.H., and Kreiner, D.C. (2020) Systems-deposits-commodities-critical minerals table
1176 for the earth mapping resources initiative. U.S. Geological Survey Open-File Report
1177 2020-1042, Reston, VA.

1178 Holloway, J.R., and Ford, C.E. (1975) Fluid-absent melting of the fluoro-hydroxy amphibole
1179 pargasite to 35 kilobars. Earth and Planetary Science Letters, 25, 44–48.

1180 Holtz, F., Dingwell, D.B., and Behrens, H. (1993) Effects of F, B_2O_3 and P_2O_5 on the solubility
1181 of water in haplogranite melts compared to natural silicate melts. Contributions to
1182 Mineralogy and Petrology, 113, 492–501.

1183 Horton, J.D., San Juan, C.A., and Stoeser, D.B. (2017) The State Geologic Map Compilation
1184 (SGMC) geodatabase of the conterminous United States, Version 1.0: Originally posted
1185 on June 30, 2017; Version 1.1: August 2017. p. 56. U.S. Geological Survey Data Series
1186 1052, Reston, VA.

Humphreys, E., Hessler, E., Dueker, K., Farmer, G.L., Erslev, E., and Atwater, T. (2003) How the Laramide-age hydration of North American lithosphere by the Farallon slab controlled subsequent activity in the western United States. International Geology Review, 45, 524–544.

Icenhower, J.P., and London, D. (1997) Partitioning of fluorine and chlorine between biotite and granitic melt: experimental calibration at 200 MPa H_2O. Contributions to Mineralogy and Petrology, 127, 17–29.

Jacob, K.H., Farmer, G.L., Buchwaldt, R., and Bowring, S.A. (2015) Deep crustal anatexis, magma mixing, and the generation of epizonal plutons in the Southern Rocky Mountains, Colorado. Contributions to Mineralogy and Petrology, 169.

Johnson, C.M., and Fridrich, C.J. (1990) Non-monotonic chemical and O, Sr, Nd, and Pb isotope zonations and heterogeneity in the mafic- to silicic-composition magma chamber of the Grizzly Peak tuff, Colorado, 105, 677–690.

Jones, C.H., Farmer, G.L., Sageman, B., and Zhong, S. (2011) Hydrodynamic mechanism for the Laramide orogeny. Geosphere, 7, 183–201.

Jones, J.V., III, Siddoway, C.S., and Connelly, J.N. (2010) Characteristics and implications of ca. 1.4 Ga deformation across a Proterozoic mid-crustal section, Wet Mountains, Colorado, USA. Lithosphere, 2, 119–135.

Keith, J.D., Shanks, W.C., Archibald, D.A., and Farrar, E. (1986) Volcanic and intrusive history of the Pine Grove porphyry molybdenum system, southwestern Utah. Economic Geology, 81, 553.

Keller, G.R., Karlstrom, K.E., Williams, M.L., Miller, K.C., Andronicos, C., Levander, A.R., Snelson, C.M., and Prodehl, C. (2005) The dynamic nature of the continental crust-mantle boundary: Crustal evolution in the southern Rocky Mountain region as an example. In K.E. Karlstrom and G.R. Keller, Eds., The Rocky Mountain Region: An Evolving Lithosphere Tectonics, Geochemistry, and Geophysics, Geophysical Monograph Series, 154, pp. 403-420. American Geophysical Union.

Kellogg, K.S., Shroba, R.R., Ruleman, C.A., Bohannon, R.G., McIntosh, W.C., Premo, W.R., Cosca, M.A., Moscati, R.J., and Brandt, T.R. (2017) Geologic map of the upper Arkansas River valley region, north-central Colorado p. 80. Scientific Investigations Map 3382, Reston, VA.

Landman, R.L., and Flowers, R.M. (2013) (U-Th)/He thermochronologic constraints on the evolution of the northern Rio Grande Rift, Gore Range, Colorado, and implications for rift propagation models. Geosphere, 9, 170–187.

Lee, C.-T.A., and Tang, M. (2020) How to make porphyry copper deposits. Earth and Planetary Science Letters, 529, 115868.

Lester, A., and Farmer, G.L. (1998) Lower crustal and upper mantle xenoliths along the Cheyenne belt and vicinity. Rocky Mountain Geology, 33, 293–304.

Liao, Y., Wei, C., and Rehman, H.U. (2021) Titanium in calcium amphibole: Behavior and thermometry. American Mineralogist, 106, 180–191.

Lipman, P.W. (2000) Central San Juan caldera cluster: Regional volcanic framework. Geological Society of America Special Papers, 346, 9–69.

1229 Lipman, P.W. (2007) Incremental assembly and prolonged consolidation of Cordilleran magma
1230 chambers: Evidence from the Southern Rocky Mountain volcanic field. Geosphere, 3,
1231 42–70.

1232 Liu, Y., Jiang, S., and Bagas, L. (2016) The genesis of metal zonation in the Weilasituo and
1233 Bairendaba Ag–Zn–Pb–Cu–(Sn–W) deposits in the shallow part of a porphyry Sn–W–Rb
1234 system, Inner Mongolia, China. Ore Geology Reviews, 75, 150–173.

1235 Liu, Y., Bagas, L., and Jiang, S. (2019) Genesis of porphyry Mo deposits linked to gradually
1236 dehydrating subcontinental lithospheric mantle metasomatised by previous subduction in
1237 northeastern China. Lithos, 336–337, 143–150.

1238 Locock, A.J. (2014) An Excel spreadsheet to classify chemical analyses of amphiboles following
1239 the IMA 2012 recommendations. Computers & Geosciences, 62, 1–11.

1240 Lüders, V., Romer, R.L., Gilg, H.A., Bodnar, R.J., Pettke, T., and Misantoni, D. (2008) A
1241 geochemical study of the Sweet Home Mine, Colorado Mineral Belt, USA: hydrothermal
1242 fluid evolution above a hypothesized granite cupola. Mineralium Deposita, 44, 415.

1243 Ludington, S., and Plumlee, G.S. (2009) Climax-type porphyry molybdenum deposits: U.S.
1244 Geological Survey Open-File Report 2009-1215, 16 p.

1245 Lundblad, S.P. (1994) Evolution of small carbonate platforms in the Umbria-Marche Apennines,
1246 Italy, 145 p. Ph.D thesis, University of North Carolina at Chapel Hill, Chapel Hill.

1247 Manning, D.A.C. (1981) The effect of fluorine on liquidus phase relationships in the system Qz-
1248 Ab-Or with excess water at 1 kb. Contributions to Mineralogy and Petrology, 76, 206–
1249 215.

McCubbin, F.M., Vander Kaaden, K.E., Tartèse, R., Boyce, J.W., Mikhail, S., Whitson, E.S., Bell, A.S., Anand, M., Franchi, I.A., Wang, J., and others (2015) Experimental investigation of F, Cl, and OH partitioning between apatite and Fe-rich basaltic melt at 1.0–1.2 GPa and 950–1000 °C. American Mineralogist, 100, 1790–1802.

McIntosh, W.C., and Chapin, C.E. (2004) Geochronology of the central Colorado volcanic field. New Mexico Bureau of Geology & Mineral Resources Bulletin, 160, 205–237.

Mercer, C.N., Hofstra, A.H., Todorov, T.I., Roberge, J., Burgisser, A., Adams, D.T., and Cosca, M. (2015) Pre-eruptive conditions of the Hideaway Park Topaz Rhyolite: Insights into metal source and evolution of magma parental to the Henderson porphyry Molybdenum deposit, Colorado. Journal of Petrology, 56, 645–679.

Mills, R.D. (2012) Re-evaluating pluton/volcano connections and igneous textures in light of incremental magma emplacement. 99 p. Ph.D thesis, University of North Carolina at Chapel Hill, Chapel Hill.

Mills, R.D., and Coleman, D.S. (2013) Temporal and chemical connections between plutons and ignimbrites from the Mount Princeton magmatic center. Contributions to Mineralogy and Petrology, 165, 961–980.

Mills, R.D., Simon, J.I., and DePaolo, D.J. (2018) Calcium and neodymium radiogenic isotopes of igneous rocks: Tracing crustal contributions in felsic magmas related to super-eruptions and continental rifting. Earth and Planetary Science Letters, 495, 242–250.

Morrison, J. (1991) Compositional constraints on the incorporation of Cl into amphiboles. American Mineralogist, 76, 1920–1930.

Moyen, J.-F. (2009) High Sr/Y and La/Yb ratios: The meaning of the "adakitic signature." Lithos, 112, 556–574.

Munoz, J.L. (1984) F-OH and Cl-OH exchange in micas with applications to hydrothermal ore deposits. In S.W. Bailey, Ed., Micas, pp. 469-491. Mineralogical Society of America.

Moore, G., Vennemann, T., and Carmichael, I.S.E. (1998) An empirical model for the solubility of H_2O in magmas to 3 kilobars. American Mineralogist, 83, 36–42.

Mutschler, F.E., Larson, E.E., and Bruce, R.M. (1987) Laramide and younger magmatism in Colorado - new petrologic and tectonic variations on old themes. Colorado School of Mines Quarterly, 82, 1–47.

Nijland, T.G., Jansen, J.B.H., and Maijer, C. (1993) Halogen geochemistry of fluid during amphibolite-granulite metamorphism as indicated by apatite and hydrous silicates in basic rocks from the Bamble Sector, South Norway. Lithos, 30, 167–189.

Oberti, R., Ungaretti L., Cannillo E., and Hawthorne, F.C. (1992) The behaviour of Ti in amphiboles. I. Four- and six-coordinated Ti in richterite. European Journal of Mineralogy, 3, 425-439.

O'Neill, J.M. (1981) Geologic map of the Mt. Richthofen Quadrangle and the western part of the Fall River Pass Quadrangle, Grand and Jackson Counties, Colorado. U.S. Geological Survey Miscellaneous Investigations Series Map I-1291.

O'Neill, L.C., Elliott, B.A., and Kyle, J.R. (2017) Mineralogy and crystallization history of a highly differentiated REE-enriched hypabyssal rhyolite: Round Top laccolith, Trans-Pecos, Texas. Mineralogy and Petrology, 111, 569–592.

Ouyang, H., Mao, J., and Hu, R. (2020) Geochemistry and crystallization conditions of magmas related to porphyry Mo mineralization in northeastern China. Economic Geology, 115, 79–100.

Parrish, R.R., and Krogh, T.E. (1987) Synthesis and purification of ^{205}Pb for U/Pb geochronology. Chemical Geology: Isotope Geoscience section, 66, 103–110.

Pearson, R.C., Braddock, W.A., Flanigan, V.J., and Patten, L.L. (1981) Mineral resources of the Comanche-Big South, Neota-Flat Top, and Never Summer Wilderness study areas, north-central Colorado: U.S. Geological Survey Open-File Report 81-578.

Pettke, T., Oberli, F., and Heinrich, C.A. (2010) The magma and metal source of giant porphyry-type ore deposits, based on lead isotope microanalysis of individual fluid inclusions. Earth and Planetary Science Letters, 296, 267–277.

Putirka, K.D. (2008) Thermometers and barometers for volcanic systems. Reviews in Mineralogy and Geochemistry, 69, 61-120.

Rosenberg, P.E., and Foit, F.F. (1977) Fe^{2+} -F avoidance in silicates. Geochimica et Cosmochimica Acta, 41, 345–346.

Rosera, J.M., Coleman, D.S., and Stein, H.J. (2013) Re-evaluating genetic models for porphyry Mo mineralization at Questa, New Mexico; implications for ore deposition following silicic ignimbrite eruption. Geochemistry, Geophysics, Geosystems, 14, 787–805.

Rosera, J.M., Gaynor, S.P., and Coleman, D.S. (2021) Spatio-temporal shifts in magmatism and mineralization in northern Colorado beginning in the Late Eocene. Economic Geology, 116, 987-1010.

Rudnick, R.L., and Gao, S. (2003) 3.01 - Composition of the Continental Crust. In H.D. Holland and K.K. Turekian, Eds., Treatise on Geochemistry pp. 1–64. Pergamon, Oxford.

Sajeev, K., Osanai, Y., Kon, Y., and Itaya, T. (2009) Stability of pargasite during ultrahigh-temperature metamorphism: A consequence of titanium and REE partitioning? American Mineralogist, 94, 535–545.

Selverstone, J., Pun, A., and Condie, K.C. (1999) Xenolithic evidence for Proterozoic crustal evolution beneath the Colorado Plateau. Geological Society of America Bulletin, 111, 590–606.

Shu, Q., and Chiaradia, M. (2021) Mesozoic Mo Mineralization in northeastern China did not require regional-scale pre-enrichment. Economic Geology, 116, 1227-1237.

Simmons, E.C., and Hedge, C.E. (1978) Minor-element and Sr-isotope geochemistry of Tertiary stocks, Colorado mineral belt. Contributions to Mineralogy and Petrology, 67, 379–396.

Skjerlie, K.P., and Johnston, A.D. (1993) Fluid-absent melting behavior of an F-rich tonalitic gneiss at mid-crustal pressures: Implications for the generation of anorogenic granites. Journal of Petrology, 34, 785–815.

Snelson, C.M., Keller, G.R., Miller, K.C., Rumpel, H.M., and Prodehl, C. (2005) Regional crustal structure derived from the CD-ROM 99 seismic refraction/wide-angle reflection profile: The lower crust and upper mantle. In K.E. Karlstrom and G.R. Keller, Eds., The Rocky Mountain Region: An Evolving Lithosphere Tectonics, Geochemistry, and Geophysics, Geophysical Monograph Series, 154, pp. 271-291. American Geophysical Union.

1334 Spear, F.S. (1981) An experimental study of hornblende stability and compositional variability in
1335 amphibolite. American Journal of Science, 281, 697–734.

1336 Stacey, J.S., and Kramers, J.D. (1975) Approximation of terrestrial lead isotope evolution by a
1337 two-stage model. Earth and Planetary Science Letters, 26, 207–221.

1338 Stein, H.J. (1985) A lead, strontium, and sulfur isotope study of the Laramide-Tertiary intrusions
1339 and mineralization in the Colorado Mineral Belt with emphasis on Climax-type porphyry
1340 molybdenum systems plus a summary of other newly acquired isotopic and rare earth
1341 element data, 493 p. Ph.D dissertation, University of North Carolina at Chapel Hill,
1342 Chapel Hill, NC.

1343 Stein, H.J., and Crock, J.G. (1990) Chapter 11: Late Cretaceous-Tertiary magmatism in the
1344 Colorado Mineral Belt; Rare earth element and samarium-neodymium isotopic studies.
1345 Geological Society of America Memoirs, 174, 195–224.

1346 Sun, Y., Teng, F.-Z., Pang, K.-N., Ying, J.-F., and Kuehner, S. (2021) Multistage mantle
1347 metasomatism deciphered by Mg−Sr−Nd−Pb isotopes in the Leucite Hills lamproites.
1348 Contributions to Mineralogy and Petrology, 176, 45.

1349 Toulmin III, P., and Hammarstrom, J.M. (1990) Geology of the Mount Aetna volcanic center,
1350 Chaffee and Gunnison Counties, Colorado. U.S. Geological Survey Bulletin 1864.

1351 Tsunogae, T., Osanai, Y., Owada, M., Toyoshima, T., Hokada, T., and Crowe, W. (2003) High
1352 fluorine pargasites in ultrahigh temperature granulites from Tonagh Island in the Archean
1353 Napier Complex, East Antarctica. Lithos, 70, 21–38.

1354 Tweto, O. (1975) Laramide (Late Cretaceous - Early Tertiary) Orogeny in the Southern Rocky
1355 Mountains. In B.F. Curtis, Ed., Cenozoic history of the Southern Rocky Mountains.
1356 Geological Society of America Memoir 144. pp. 1–44.

1357 Tweto, O. (1979) The Rio Grande Rift system in Colorado. In R. E. Riecker, Ed., Rio Grande
1358 Rift: Tectonics and Magmatism. pp. 33-56. American Geophysical Union, USA.

1359 Tweto, O., and Sims, P.K. (1963) Precambrian ancestry of the Colorado Mineral Belt.
1360 Geological Society of America Bulletin, 74, 991.

1361 Van den Bleeken, G., and Koga, K.T. (2015) Experimentally determined distribution of fluorine
1362 and chlorine upon hydrous slab melting, and implications for F–Cl cycling through
1363 subduction zones. Geochimica et Cosmochimica Acta, 171, 353–373.

1364 Van Loenen, R.E., Lee, G.K., Campbell, D.L., and Thompson, J.R. (1989) Mineral resource
1365 potential of Mount Massive Wilderness, Lake County, Colorado. U.S. Geological Survey
1366 Bulletin 1636.

1367 Wallace, A.R. (1995) Isotopic geochronology of the Leadville 1 degree x 2 degrees Quadrangle,
1368 west-central Colorado; summary and discussion. U.S. Geological Survey Bulletin 2104.

1369 Webster, J.D., Baker, D.R., and Aiuppa, A. (2018) Halogens in Mafic and Intermediate-Silica
1370 Content Magmas. In D.E. Harlov and L. Aranovich, Eds., The Role of Halogens in
1371 Terrestrial and Extraterrestrial Geochemical Processes: Surface, Crust, and Mantle pp.
1372 307–430. Springer International Publishing, Cham.

White, W.H., Bookstrom, A.A., Kamilli, R.J., Ganster, M.W., Smith, R.P., Ranta, D.E., and Steininger, R.C. (1981) Character and origin of Climax-type molybdenum deposits. Economic Geology, 75th anniversary volume, 270–316.

Zhao, Q., Zhai, D., Mathur, R., Liu, J., Selby, D., and Williams-Jones, A.E. (2021) The giant Chalukou porphyry Mo deposit, northeast China: The product of a short-lived, high flux mineralizing event. Economic Geology.

Zhang, C., Li, X., Behrens, H., and Holtz, F. (2022) Partitioning of OH-F-Cl between biotite and silicate melt: Experiments and an empirical model. Geochimica et Cosmochimica Acta, 317, 155–179.

Zimmerer, M.J., and McIntosh, W.C. (2012) An investigation of caldera-forming magma chambers using the timing of ignimbrite eruptions and pluton emplacement at the Mt. Aetna caldera complex. Journal of Volcanology and Geothermal Research, 245–246, 128–148.

FIGURE CAPTIONS

Figure 1. Maps showing the location of study area, as well as simplified geology. **(a)** Generalized map showing the location of the Colorado Mineral Belt, Cenozoic F-rich silicic rocks, and the State Line diatreme district. Blue outlines mark approximate extent of maps shown in panels (b) and (c). **(b)** Simplified geological map showing the Never Summer batholith, silicic dikes, and sampling sites used in this study. Faults are dashed where they are inferred and/or concealed. Map modified after O'Neill (1981). Triangles indicate sample locations, and those with sample number labels were selected for biotite EMP analysis. **(c)** Simplified geological map of the central Colorado Mineral Belt and sample sites. Thin dashed ovals show

approximate extent of historical and active mining districts in the area. Modified after Horton et al. (2017). Colored point symbols represent sample locations (see Table S3 for sample summaries and coordinates). BC – Brown's Canyon district, C – Climax Mo deposit, GPC – Grizzly Peak caldera, H – Henderson Mo deposit; MAC – Mount Aetna caldera, ME – Mount Emmons Mo deposit, MP – Montezuma pluton, MPB – Mount Princeton batholith, Q – Questa Mo deposit, TLP – Twin Lakes pluton.

Figure 2. Select plots showing amphibole compositions from two-pyroxene mafic granulite xenoliths of the State Line diatreme district. **(a)** Nomenclature for Ca amphibole after Hawthorne et al. (2012) and Locock (2014). **(b)** F versus Cl in wt% showing a positive correlation between abundance of Cl and F in amphibole. **(c)** Cl (in apfu) versus $Fe^{2+}/(Fe^{2+} + Mg)$ showing a weak positive correlation. **(d)** F versus K (both in apfu). Note that sample SD2-LC78 is an outlier. Dashed field shows amphibole compositions from the ultrahigh temperature (UHT) Highland Complex in Sri Lanka (Sajeev et al. 2009). **(e)** Ti versus ^{IV}Al. Dashed field as in panel (c). Lower crust xenolith literature data from Selverstone et al. (1999) and Farmer et al. (2005); mafic high-grade metamorphic rock data from Nijland et al. (1993), Tsunogae et al. (2003), and Sajeev et al. (2009).

Figure 3. Plots showing estimated temperature and pressure equilibration conditions for amphibole from garnet-free mafic granulite xenoliths from the State Line District. Red color fill in each panel includes all analyses other than those from SD2-LC78 (four samples; see Fig. 2). Top panel: kernel density estimates of temperatures calculated from the Ti in calcium amphibole thermometer (Liao et al. 2021). Bottom panel: plot showing isopleths of TiO_2 (solid lines) and Al_2O_3 (dashed lines) in *P-T* space after Ernst and Liu (1998). Colored boxes correspond to range of values measured in amphiboles from the State Line two-pyroxene mafic granulites. For

comparison, the *P-T* range estimated for peak metamorphism of garnet-bearing lithologies from the State Line District are overlain (gray box; Farmer et al. 2005).

Figure 4. Select plots showing the composition of biotite from the Never Summer batholith. **(a)** Biotite quadrilateral; Fe / (Fe + Mg) versus total Al, all in apfu. Light blue fields with dashed outlines correspond to other topaz rhyolites from the western United States (after Christiansen et al. 2007). Italicized biotite end member names correspond to their closest corner on the quadrilateral. **(b)** log(Cl/OH) versus $X_{phlogopite}$. **(c)** Ti versus Mg/(Mg + Fe_{total}) modified after Henry et al. (2005). Gray curves show Ti in biotite isotherms, which are only calibrated above Mg(Mg + Fe_{total}) > 0.25 (vertical dashed line; Henry et al. 2005) and have been modified to 11O + 2^{W}(OH, F, Cl, O) biotite normalization. **(d)** log(F/OH) versus $X_{phlogopite}$. Note that log(F/OH) in Mount Cumulus increases for decreasing $X_{phlogopite}$ across samples, which is opposite of the Fe-F avoidance principle. The Mount Cumulus biotite from samples 10-KJ-MC-94 and 10-KJ-MC-91 have unusually low $X_{phlogopite}$ and are from whole-rock samples with < 5 ppm Sr (see Fig. 6a).

Figure 5. Select major element variation diagrams versus wt% silica for samples analyzed in this study (large symbols) as well as other Cretaceous and younger rocks from northern Colorado (small symbols). Samples are broadly color-coded by tectono-magmatic groups discussed in text. **(a)** Molar $Al_2O_3/(Na_2O + K_2O)$ versus SiO_2 (wt%) shows that most samples are peraluminous (horizontal dashed line marks peraluminous/metaluminous boundary). **(b)** $FeO_{tot}/(FeO_{tot} + MgO)$ versus SiO_2 scatterplot showing that many of pre-extensional rocks are magnesian (i.e., below the grey line, after Frost et al. 2001). Rift-related leucogranites and rhyolites, as well as aplites associated with the Twin Lakes and Montezuma plutons, are also ferroan. **(c)** $Na_2O + K_2O$ (in wt%) versus SiO_2 showing silicic rocks associated with extension tend to have higher alkali contents than older igneous rocks. Extrusive total alkali-silica classification shown for reference

only; note that many samples are intrusive. Literature data sources are: Simmons and Hedge (1978), Farmer and DePaolo (1984), Stein (1985), Bailley (2010), and Jacob et al. (2015). CMB – Colorado Mineral Belt.

Figure 6. Trace element abundance and ratio variation diagrams. Symbols as in Figure 5. **(a)** Sr vs. SiO_2 showing strongly depleted Sr abundances in rift-related leucogranites, rhyolites, older aplites, and the Alma district rhyolites. Note that portions of Mount Cumulus contain < 5 ppm Sr. **(b)** Rb vs. SiO_2 showing a weak positive correlation between log(Rb) and silica content. **(c)** Nb vs. SiO_2 showing distinct contrast between extension-related rocks and early magma centers. **(d)** Y vs. SiO_2 showing similar patterns similar to Nb versus SiO_2. **(e)** Variation of Rb/Sr (note log scale) versus SiO_2 showing a positive curvilinear relationship. Extension-related silicic rocks have the highest Rb/Sr values. **(f)** Variation of Sr/Y versus SiO_2 showing relatively high Sr/Y (>40) of Laramide suite and low Sr/Y for extension-related leucogranites and rhyolites.

Figure 7. Lead isotopic variation diagrams for samples from this study as well as other Cretaceous and younger igneous rocks from central and northern Colorado. Symbols as in Figure 5. **(a,c)** $^{206}Pb/^{204}Pb$ and $^{208}Pb/^{204}Pb$ variation in comparison to SiO_2. **(b,d)** Initial $^{206}Pb/^{204}Pb$-$^{207}Pb/^{204}Pb$ and $^{206}Pb/^{204}Pb$-$^{208}Pb/^{204}Pb$ plots showing central and northern Colorado igneous rocks relative to growth curve after Stacey and Kramers (1975; SK, solid gray line), one of the proposed curves for the subcontinental lithospheric mantle beneath much of the western United States (CLM, dashed line; Pettke et al. 2010), and the northern hemisphere reference line (NHRL; Hart 1984). Black numbers and boxes along growth curves correspond to age, in Ga. Gray field outlines felsic Proterozoic rocks whose isotopic compositions are corrected to 35 Ma (Frazer 2017). Most of the data fall between the SK and CLM model curves. Dark gray outline corresponds to rocks located in the northern Colorado Mineral Belt (including the Montezuma

pluton, after Stein 1985) and Never Summer igneous complex. Dashed blue polygon highlights samples from the central and southern Colorado Mineral Belt, which tend to have less radiogenic $^{206}Pb/^{204}Pb_i$ compositions. Samples associated with F-rich porphyry Mo mineralization are highlighted in pink in panel d (data from this study and Stein 1985). Note that two samples from the Alma district with highly radiogenic Pb isotopic compositions are not included in these plots (see Table S5).

Figure 8. Strontium isotopic variation diagrams. **(a)** $^{87}Sr/^{86}Sr_i$ versus SiO_2 diagram showing that the two Alma rhyolites, as well as the Turquoise Lake porphyry, have highly radiogenic Sr (>0.715). Most of the intermediate samples from Twin Lakes through Breckenridge have $^{87}Sr/^{86}Sr$ <0.708 and samples from the Montezuma complex have slightly more radiogenic Sr. Horizontal dashed line in panel a shows limit of ordinate axes for the same plot in panel **(b)**. Symbols as in Figure 5. CMB – Colorado Mineral Belt.

Figure 9. Initial εNd versus SiO_2 variation diagram, showing no strong correlation between Nd isotopic composition and silica content. Symbols as in Figure 5.

Figure 10. Back-scattered electron image of amphibole (analysis 4) from sample NX4-LC2. This xenolith contains plagioclase that is variably altered to clay, but this effect showed no influence on amphibole measurements (two examples of alteration are highlighted by dashed blue lines). Bright minerals located around grain boundaries are mostly barite that was introduced by host kimberlite (see text). Amphibole (amph) show no significant disequilibrium textures or obvious zonations. opx – orthopyroxne, cpx – clinopyroxne, plag – plagioclase (black and gray areas).

Figure 11. Histograms and variation diagrams showing Sr and Nd isotopic compositions in comparison to Proterozoic country rocks (Proterozoic rocks corrected to 35 Ma, all other samples

corrected to their initial ages). **(a)** εNd versus $^{87}Sr/^{86}Sr$ for Cenozoic and younger igneous rocks in the study area. Dashed box shows area of panel (b). Colored fields are simplified outlines of country rocks, as represented by felsic and mafic xenoliths from the Four Corners area, felsic rocks from the surface, and mafic granulite xenoliths from the State Line District. Histograms above and to the right of panel a show distribution of country rock data for Sr (top) and Nd (right). Notice that most of the felsic country rocks have $\varepsilon Nd_{35\ Ma} < -10$. **(b)** As in panel (a) but in a smaller area to show more detail. Ellipse encloses 66 Ma Windy Gap basalts. for comparison to mafic xenoliths from the region. CMB – Colorado Mineral Belt.

Figure 12. Initial $^{206}Pb/^{204}Pb$ isotopic compositions through time. **(a)** $^{206}Pb/^{204}Pb_i$ through time for samples from the Colorado Mineral Belt. Gray boxes and arrows highlight locations where younger magmas shift towards less radiogenic Pb compositions. **(b)** Same as panel (a), but only showing data for the Never Summer batholith. Two silicic dikes from the northern portion of the magma system have slightly more radiogenic $^{206}Pb/^{204}Pb_i$ than most of the samples from the Mount Cumulus leucogranite. Symbols as in Figure 5. MA – Mount Antero, MP – Mount Princeton.

Figure 13. Plots showing estimated concentrations of F and Cl in equilibrium with biotite for the Never Summer batholith samples at: **(a)** 50 MPa, and **(b)** 100 MPa. In both cases, the estimated F and Cl from biotite-melt exchange formulations are compared to batch melting models (gray curves) of garnet-free mafic lower crust using xenolith data. Labeled circles along batch melt models represent fraction melted. Gray boxes show extent of F and Cl concentrations measured in melt inclusions from Audétat (2015) and Mercer et al. (2015). Also shown for comparison are estimated average F and Cl melt concentrations from Mount Antero leucogranites (using data from Toulmin and Hammarstrom 1990: note they analyzed biotite from different samples than

the whole rock data). Gray stars denote minimum F and Cl concentrations in xenoliths that were used as starting compositions for batch melt models. Black star shows average mafic lower crust, for reference (Rudnick and Gao 2003). Arrows show fractional crystallization models for H_2O-saturated (blue arrows) and H_2O-undersatured conditions (black arrow). Length of arrow corresponds to 0.2 melt fraction remaining. Partition coefficients for batch melting and H_2O-undersaturated fractional crystallization models are shown in Table S7. H_2O-saturated models are after Candela (1986).

Figure 14. Cartoon model depicting how deep mafic crust potentially controlled F-enrichment of silicic anatectic melts in central and northern Colorado from the Cretaceous through the Oligocene. Left side of diagram depicts a lower flux of mantle derived melt and fluids (smaller black arrow) and in turn lower heat flux into garnet-free mafic lower crust. Fluorine-rich pargasite are likely to remain stable at a lower heat flux, hence the anatectic products will not be enriched in F. Right side shows higher mantle melt and fluid fluxes, perhaps during extension or caldera-forming magma events. The higher heat flux in the garnet-free mafic lower crust allows for the breakdown of F-rich pargasite observed in xenoliths, thereby producing F-rich melts that can differentiate towards leucogranitic compositions. Model modified after Mercer et al. (2015) and Jacob et al. (2015).

TABLE 1. GENERAL SUMMARY OF CRETACEOUS TO OLIGOCENE IGNEOUS ROCKS IN CENTRAL COLORADO

Tectono-Magmatic Group	Major Lithology	$^{87}Sr/^{86}Sr_i$	εNd_i	Examples
Laramide to start of flare-up (75 to 38Ma)	Monzonite	0.705 to 0.708 (mostly < 0.706)	-1 to -9	Empire stock
	Gd to Qtz Monz.	0.706 to 0.7089	-5 to – 10	Twin Lakes pluton; Montezuma pluton
Transition (37.3 to 30 Ma)	Qtz Monz. to Gr	0.707 to 0.710	-7 to -10	**Middle Mountain porphyry**; Mount Princeton batholith
Extension and Rio Grande rifting < 30 Ma	Gr. (bimodal suite)	0.708 to 0.735	-8 to -14 (CMB)	Mount Antero leucogranites
			-2 to -5 (NS)	**Climax porphyry system** Never Summer complex

Examples in bold are associated with Climax-type porphyry Mo mineralization.
Sources: Simmons and Hedge (1978), Farmer and DePaolo (1984), Stein and Crock (1990), and Jacob et al. (2015)
CMB – Colorado Mineral Belt; Gd – granodiorite; Qtz Monz. – quartz monzonite; Gr – granite; NS – Never Summer

TABLE 2. ESTIMATED RANGE OF F AND Cl CONCENTRATIONS OF MELT IN EQUILIBRIUM WITH BIOTITE

		50 MPa		100 MPa	
Sample	Description	F, ppm (*mean*)	Cl, ppm (*mean*)	F, ppm (*mean*)	Cl, ppm (*mean*)
10-KJ-MR-91	low-Sr Mount Cumulus granite	47000 to 65000 (*55000*)	1800 to 2600 (*2200*)	62000 to 87000 (*73000*)	2500 to 3400 (*2900*)
10-KJ-MR-94	low-Sr Mount Cumulus granite	37000 to 68000 (*50000*)	1100 to 1600 (*1300)*	50000 to 90000 (*67000*)	1400 to 2000 (*1700*)
NS17-05	Mount Cumulus	8800 to 20000 (*14000*)	2200 to 3400 (*2800*)	12000 to 26000 (*19000*)	3000 to 4500 (*3700*)
10-KJ-MR-109	Mafic Mount Richthofen	1000 to 1200 (*1100*)	19000 to 24000 (*22000*)	1400 to 1600 (*1500*)	26000 to 32000 (*30000*)
10-KJ-MR-110	Silicic Mount Richthofen	2500 to 4100 (*3200*)	5400 to 9500 (*7900*)	3500 to 5500 (*4300*)	7300 to 13000 (*11000*)

Figure 1

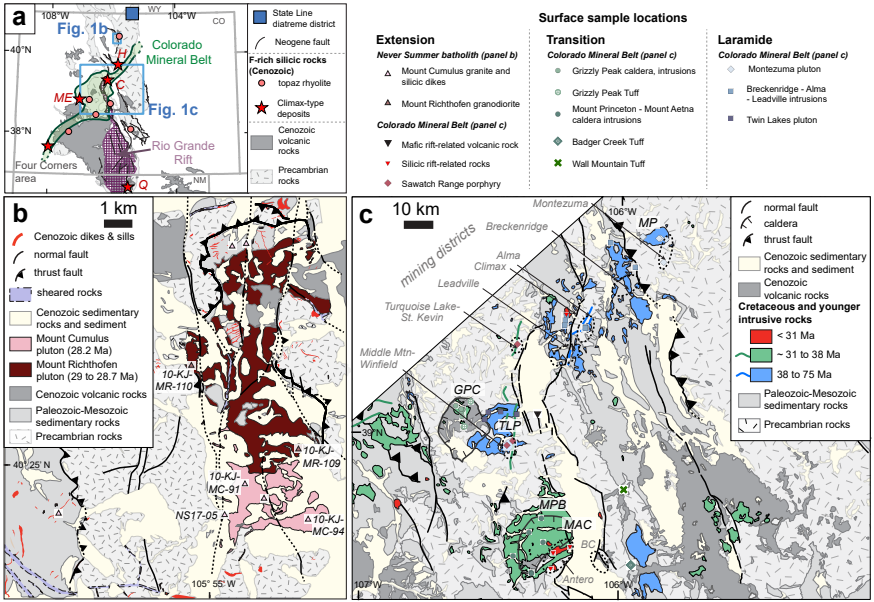
a
108°W
WY
104°W
CO
40°N
38°N
Fig. 1b
H
Colorado
Mineral Belt
ME
Fig. 1c
Rio Grande
Rift
Four Corners
area
Q
NM
State Line
diatreme district
Neogene fault
F-rich silicic rocks
(Cenozoic)
topaz rhyolite
Climax-type
deposits
Cenozoic
volcanic
rocks
Precambrian
rocks
Surface sample locations
Extension
Never Summer batholith (panel b)
Mount Cumulus granite and
silicic dikes
Mount Richthofen granodiorite
Colorado Mineral Belt (panel c)
Mafic rift-related volcanic rock
Silicic rift-related rocks
Sawatch Range porphyry
Transition
Colorado Mineral Belt (panel c)
Grizzly Peak caldera, intrusions
Grizzly Peak Tuff
Mount Princeton - Mount Aetna
caldera intrusions
Badger Creek Tuff
Wall Mountain Tuff
Laramide
Colorado Mineral Belt (panel c)
Montezuma pluton
Breckenridge - Alma
- Leadville intrusions
Twin Lakes pluton
b
1 km
Cenozoic dikes & sills
normal fault
thrust fault
sheared rocks
Cenozoic sedimentary
rocks and sediment
Mount Cumulus
pluton (28.2 Ma)
Mount Richthofen
pluton (29 to 28.7 Ma)
Cenozoic volcanic rocks
Paleozoic-Mesozoic
sedimentary rocks
Precambrian rocks
10-KJ-
MR-110
10-KJ-
MR-109
10-KJ-
MC-91
NS17-05
10-KJ-
MC-94
40° 25' N
105° 55' W
c
10 km
Montezuma
106°W
MP
Breckenridge
mining districts
Alma
Climax
Leadville
Turquoise Lake-
St. Kevin
Middle Mtn-
Winfield
GPC
TLP
MPB
MAC
BC
Antero
107°W
106°W
normal fault
caldera
thrust fault
Cenozoic sedimentary
rocks and sediment
Cenozoic
volcanic rocks
Cretaceous and younger
intrusive rocks
< 31 Ma
~ 31 to 38 Ma
38 to 75 Ma
Paleozoic-Mesozoic
sedimentary rocks
Precambrian rocks

Figure 2

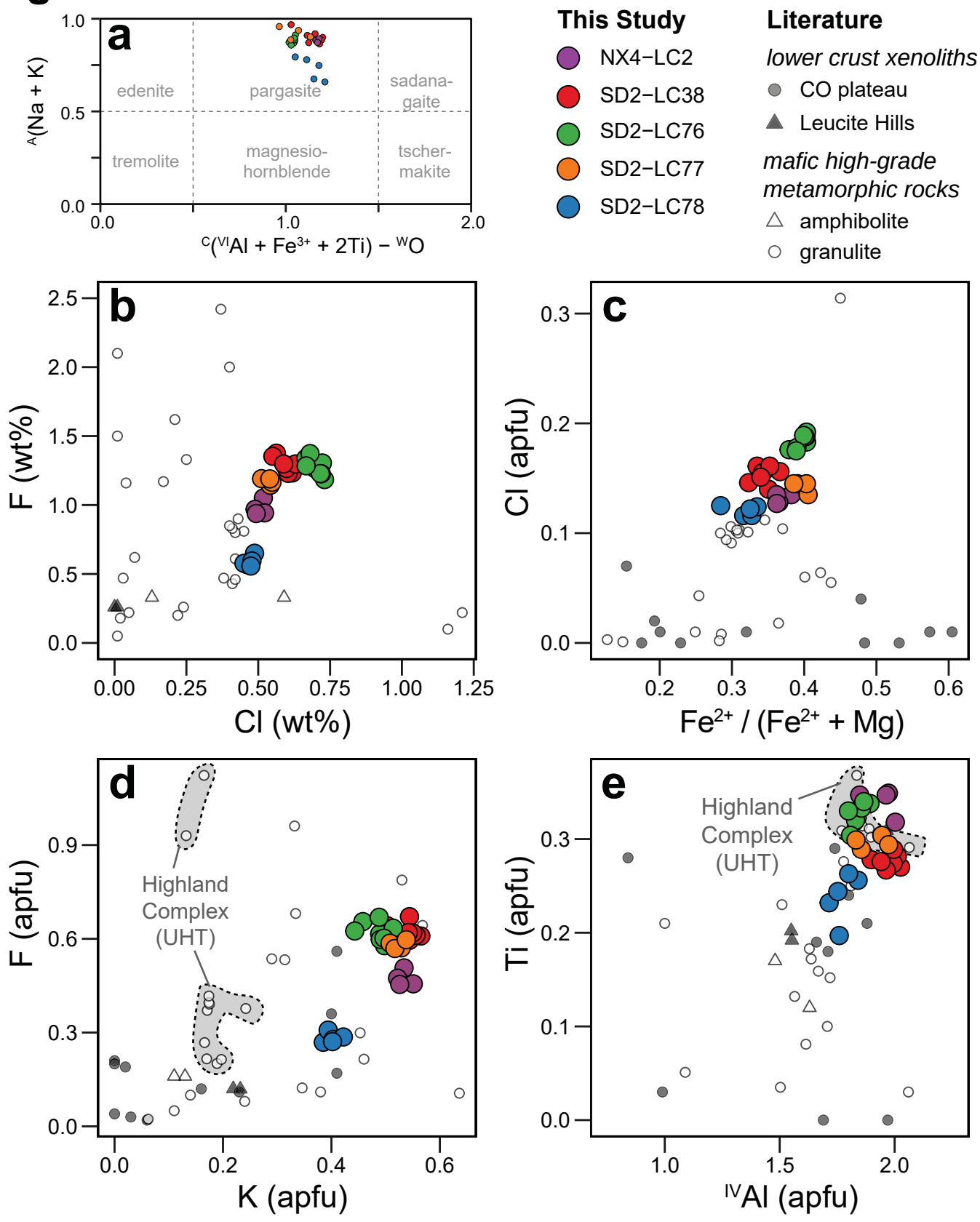
a
edenite
pargasite
sadana-
gaite
tremolite
magnesio-
hornblende
tscher-
makite
A(Na + K)
C(VIAl + Fe3+ + 2Ti) − WO
This Study
NX4−LC2
SD2−LC38
SD2−LC76
SD2−LC77
SD2−LC78
Literature
lower crust xenoliths
CO plateau
Leucite Hills
mafic high-grade
metamorphic rocks
amphibolite
granulite
b
F (wt%)
Cl (wt%)
c
Cl (apfu)
Fe2+ / (Fe2+ + Mg)
d
Highland
Complex
(UHT)
F (apfu)
K (apfu)
e
Highland
Complex
(UHT)
Ti (apfu)
IVAl (apfu)

Figure 3

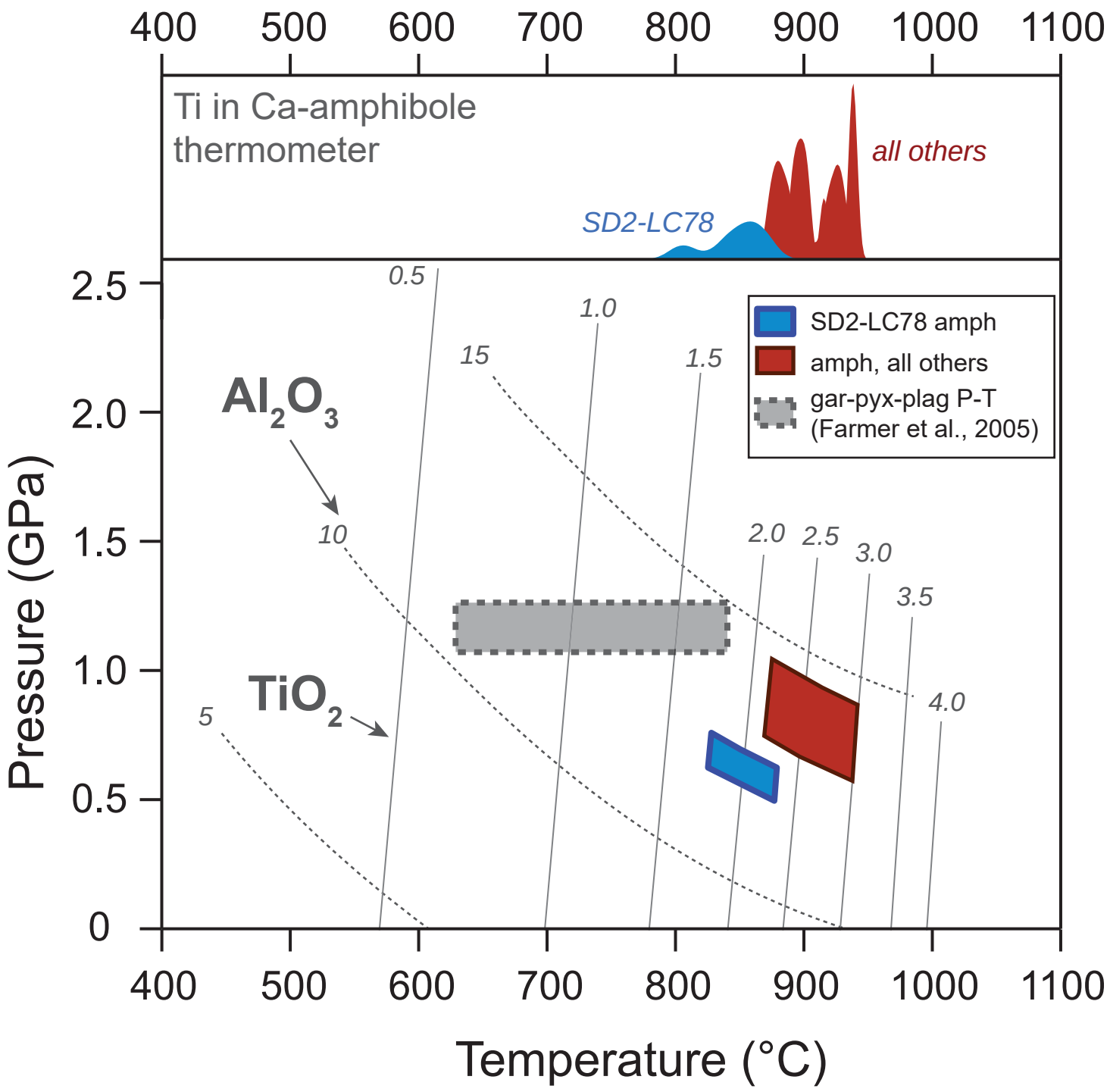
Ti in Ca-amphibole thermometer
SD2-LC78
all others
SD2-LC78 amph
amph, all others
gar-pyx-plag P-T (Farmer et al., 2005)
Al2O3
TiO2
0.5
1.0
1.5
15
10
5
2.0
2.5
3.0
3.5
4.0
Pressure (GPa)
Temperature (°C)
0
0.5
1.0
1.5
2.0
2.5
400
500
600
700
800
900
1000
1100

Figure 4

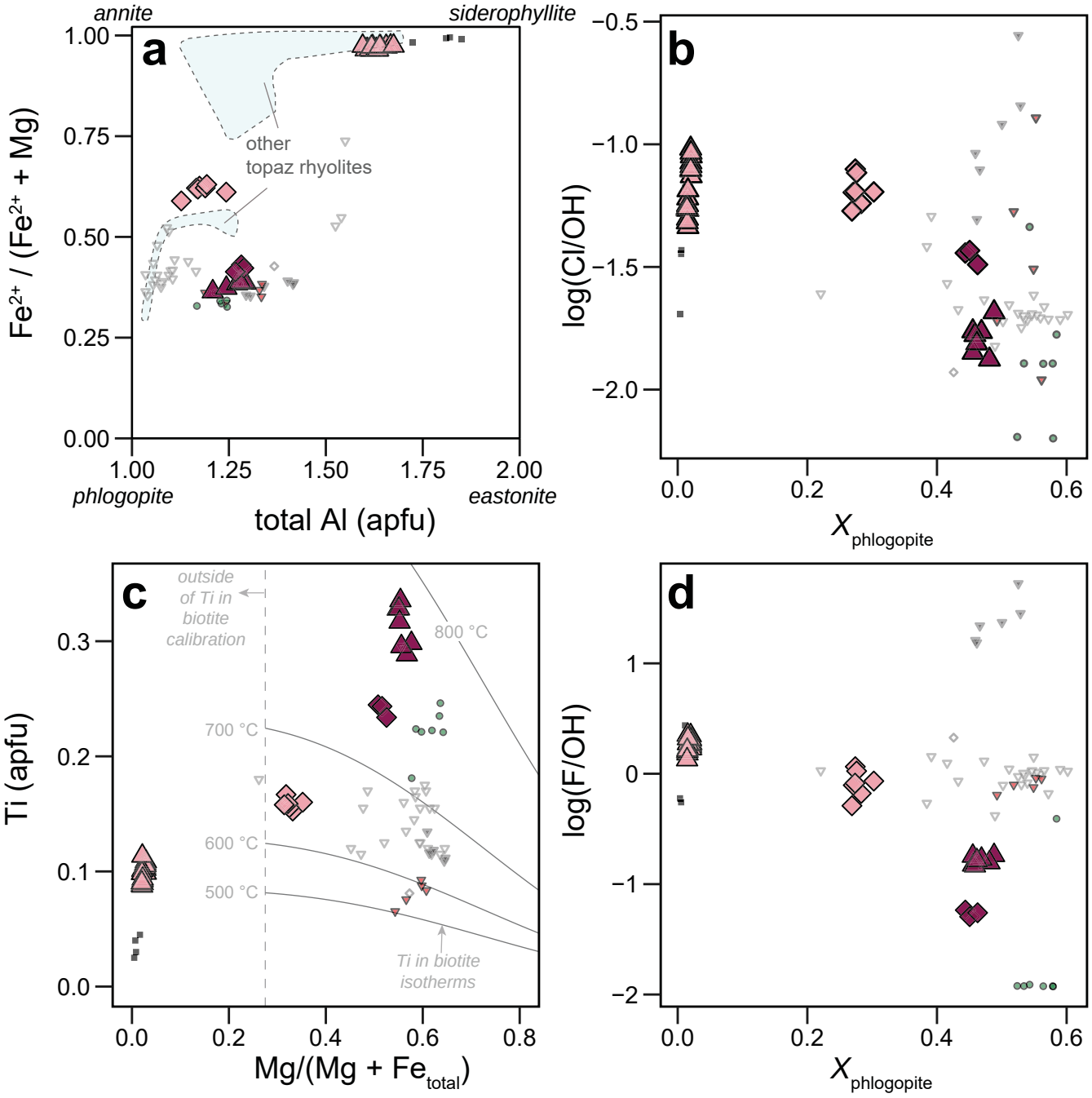

This Study

Mount Cumulus pluton

- Samples 10-KJ-MC-94 & 10-KJ-MC-91
- Baker Pass, western phase (NS17-05)

Mount Richthofen pluton

- silicic member (10-KJ-MR-110)
- mafic member (10-KJ-MR-109)

Literature

Colorado Mineral Belt

- Chalk Mountain rhyolite
- Henderson (igneous biotite)
- Hideaway Park tuff
- Mount Antero leucogranite
- Mount Princeton batholith

Other topaz rhyolite

- Honeycomb Hills (Utah)

Figure 5

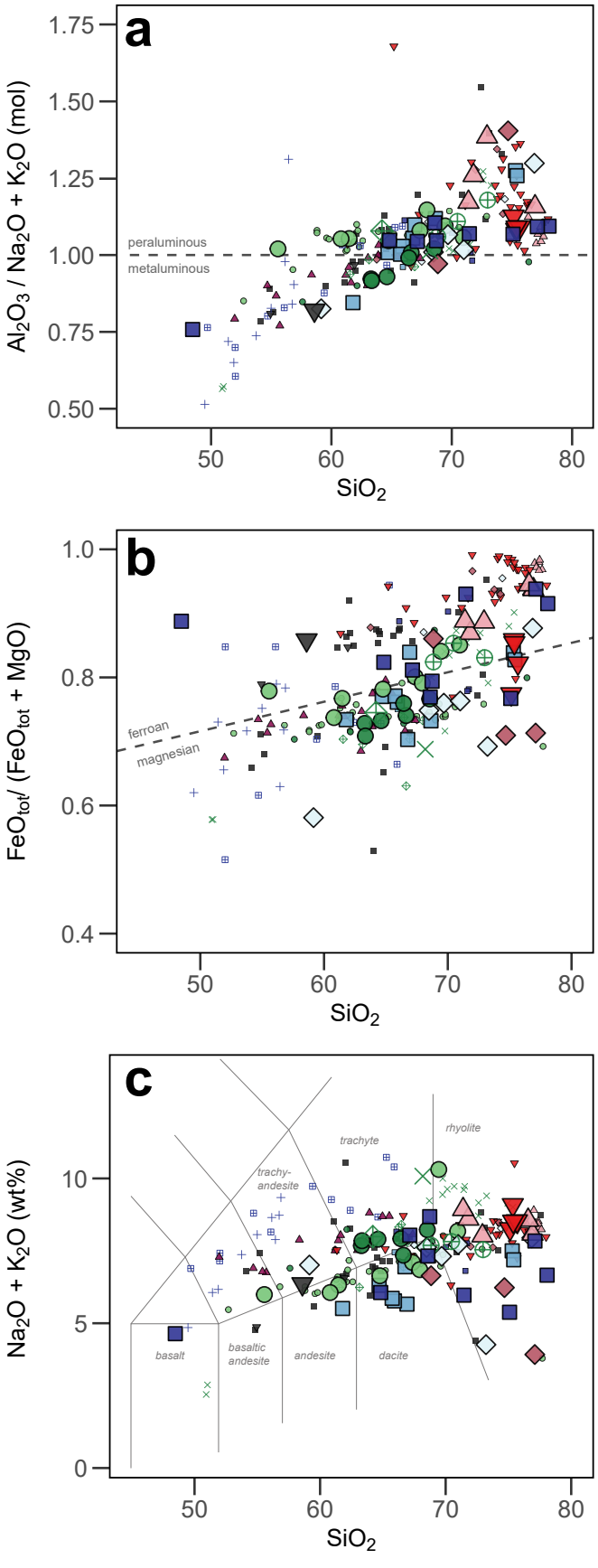

This Study

- Mafic rift-related rocks in the CMB — **Extension**
- *systems with F-rich magmas*
  - Mount Cumulus granite and silicic dikes
  - Silicic rift-related rocks in the CMB
- Sawatch Range porphyry — **Transition**
- Grizzly Peak caldera intrusions
- Grizzly Peak Tuff
- Mount Princeton − Mount Aetna caldera
- Badger Creek Tuff
- Wall Mountain Tuff
- Montezuma pluton — **Laramide**
- Breckenridge − Alma − Leadville intrusions
- Twin Lakes pluton

Literature

- Mafic rift−related rocks in the CMB — **Extension**
- Never Summer, Mount Richthofen
- *systems with F-rich magmas*
  - Mount Cumulus granite and silicic dikes
  - Silicic rift-related rocks in the CMB
- Sawatch Range porphyry — **Transition**
- Grizzly Peak caldera intrusions
- Mount Princeton − Mount Aetna intrusions
- Badger Creek Tuff
- Wall Mountain Tuff
- Montezuma pluton — **Laramide**
- Breckenridge − Alma − Leadville intrusions
- Twin Lakes pluton
- Windy Gap mafic volcanic rocks
- Monzonite suite
- Granodiorite suite, other (Laramide & Transition)

Figure 6

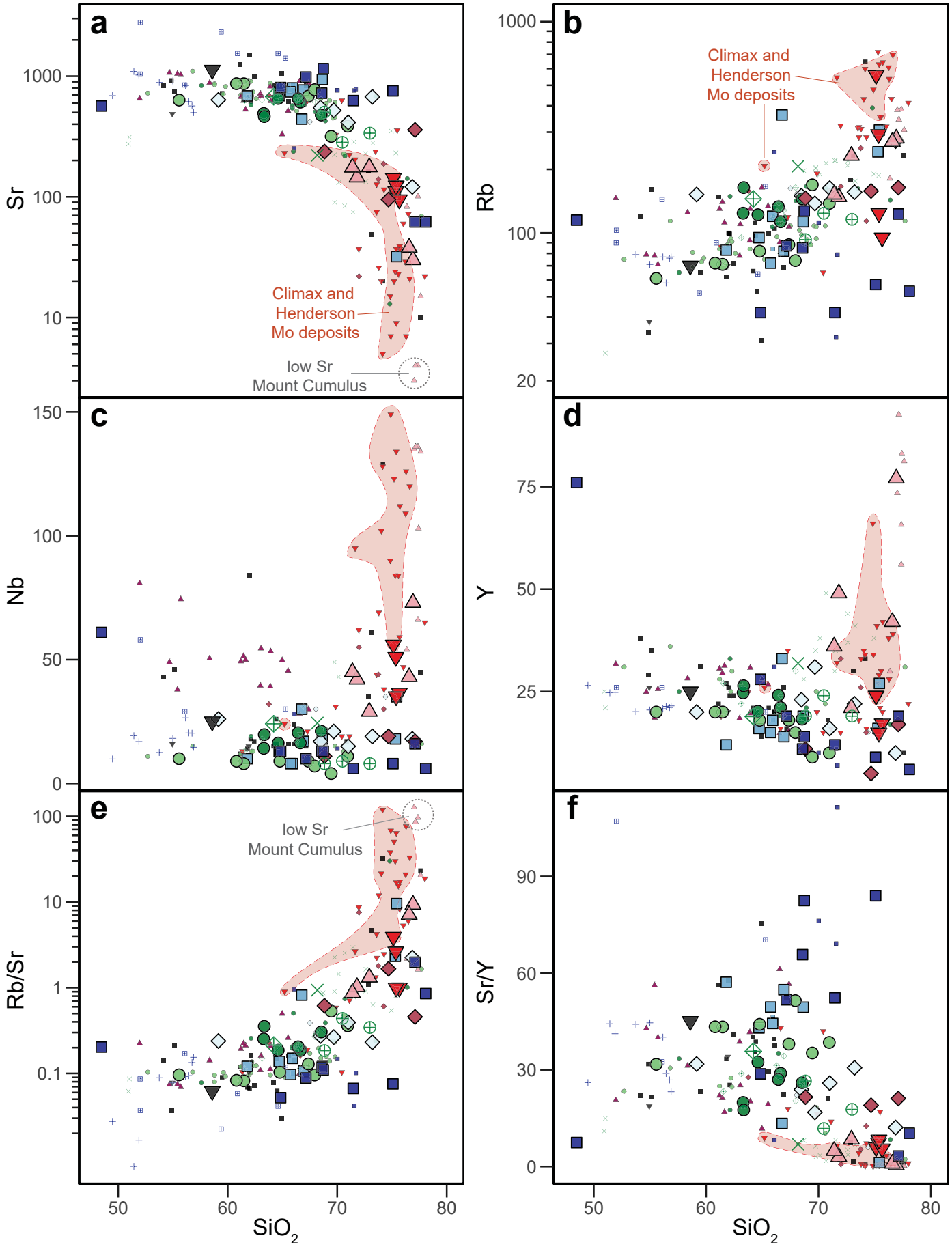
a
Sr
1000
100
10
Climax and
Henderson
Mo deposits
low Sr
Mount Cumulus
b
Rb
1000
100
20
Climax and
Henderson
Mo deposits
c
Nb
150
100
50
0
d
Y
75
50
25
e
Rb/Sr
100
10
1
0.1
low Sr
Mount Cumulus
f
Sr/Y
90
60
30
0
50
60
70
80
SiO2
SiO2

Figure 7

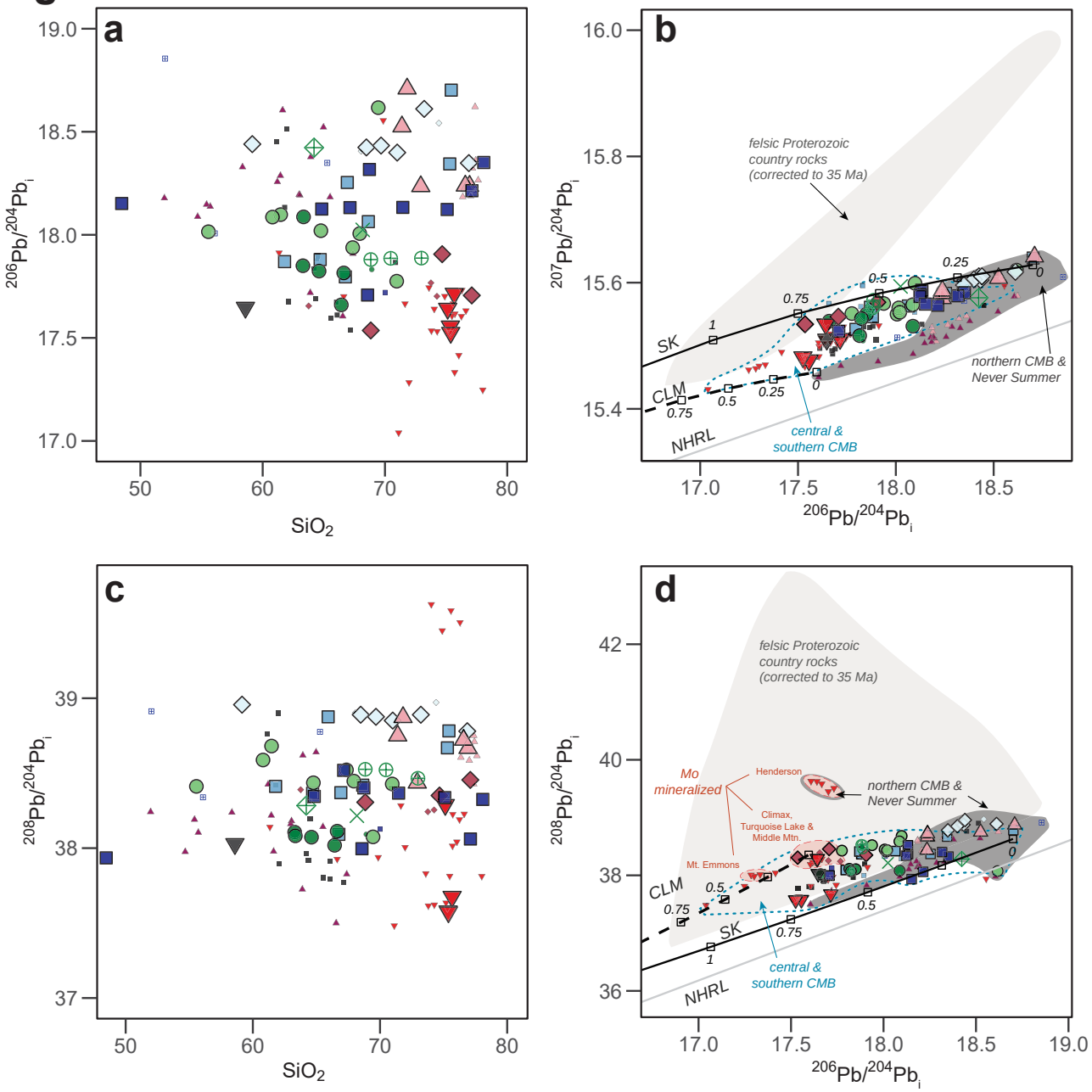

This Study

- Mafic rift-related rocks in the CMB — **Extension**
- systems with F-rich magmas:
  - Mount Cumulus granite and silicic dikes
  - Silicic rift-related rocks in the CMB
  - Sawatch Range porphyry — **Transition**
- Grizzly Peak caldera intrusions
- Grizzly Peak Tuff
- Mount Princeton – Mount Aetna caldera
- Badger Creek Tuff
- Wall Mountain Tuff
- Montezuma pluton — **Laramide**
- Breckenridge – Alma – Leadville intrusions
- Twin Lakes pluton

Literature

- Mafic rift–related rocks in the CMB — **Extension**
- Never Summer, Mount Richthofen
- systems with F-rich magmas:
  - Mount Cumulus granite and silicic dikes
  - Silicic rift-related rocks in the CMB
  - Sawatch Range porphyry — **Transition**
- Grizzly Peak caldera intrusions
- Mount Princeton – Mount Aetna intrusions
- Badger Creek Tuff
- Wall Mountain Tuff
- Montezuma pluton — **Laramide**
- Breckenridge – Alma – Leadville intrusions
- Twin Lakes pluton
- Monzonite suite
- Granodiorite suite, other

Figure 8

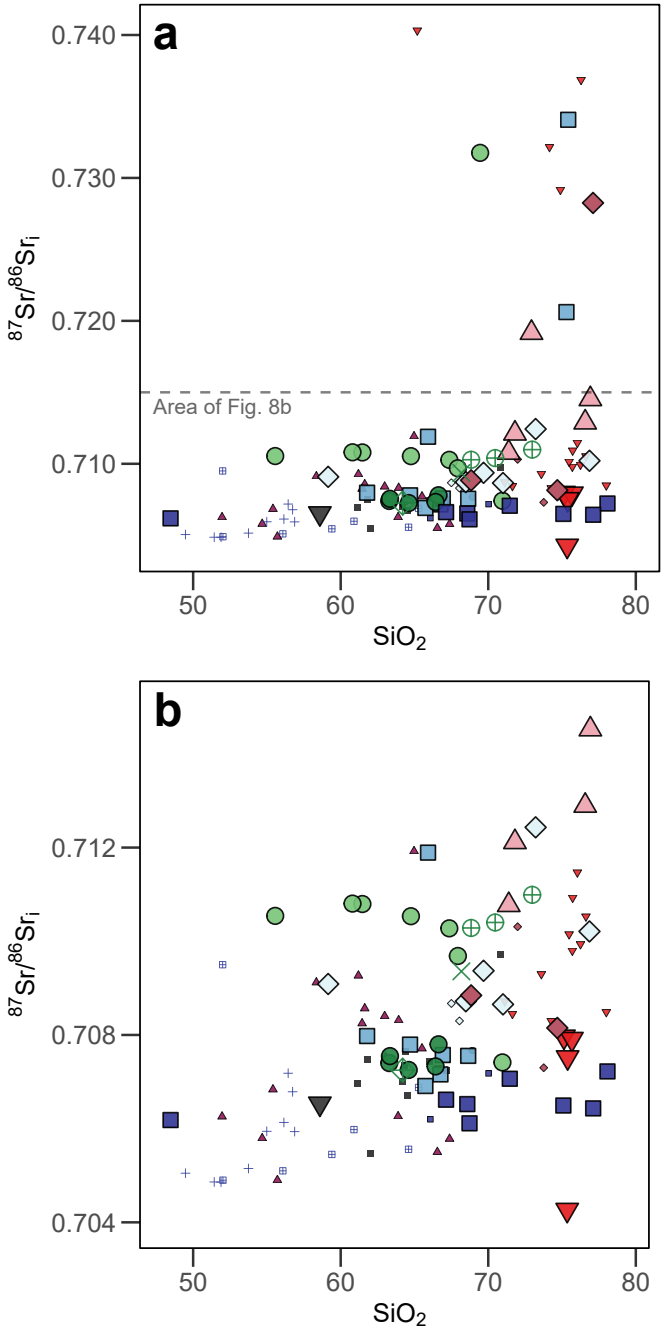
a
0.740
0.730
0.720
0.710
$^{87}Sr/^{86}Sr_i$
Area of Fig. 8b
50
60
70
80
SiO_2
b
0.712
0.708
0.704
$^{87}Sr/^{86}Sr_i$
50
60
70
80
SiO_2

Figure 9

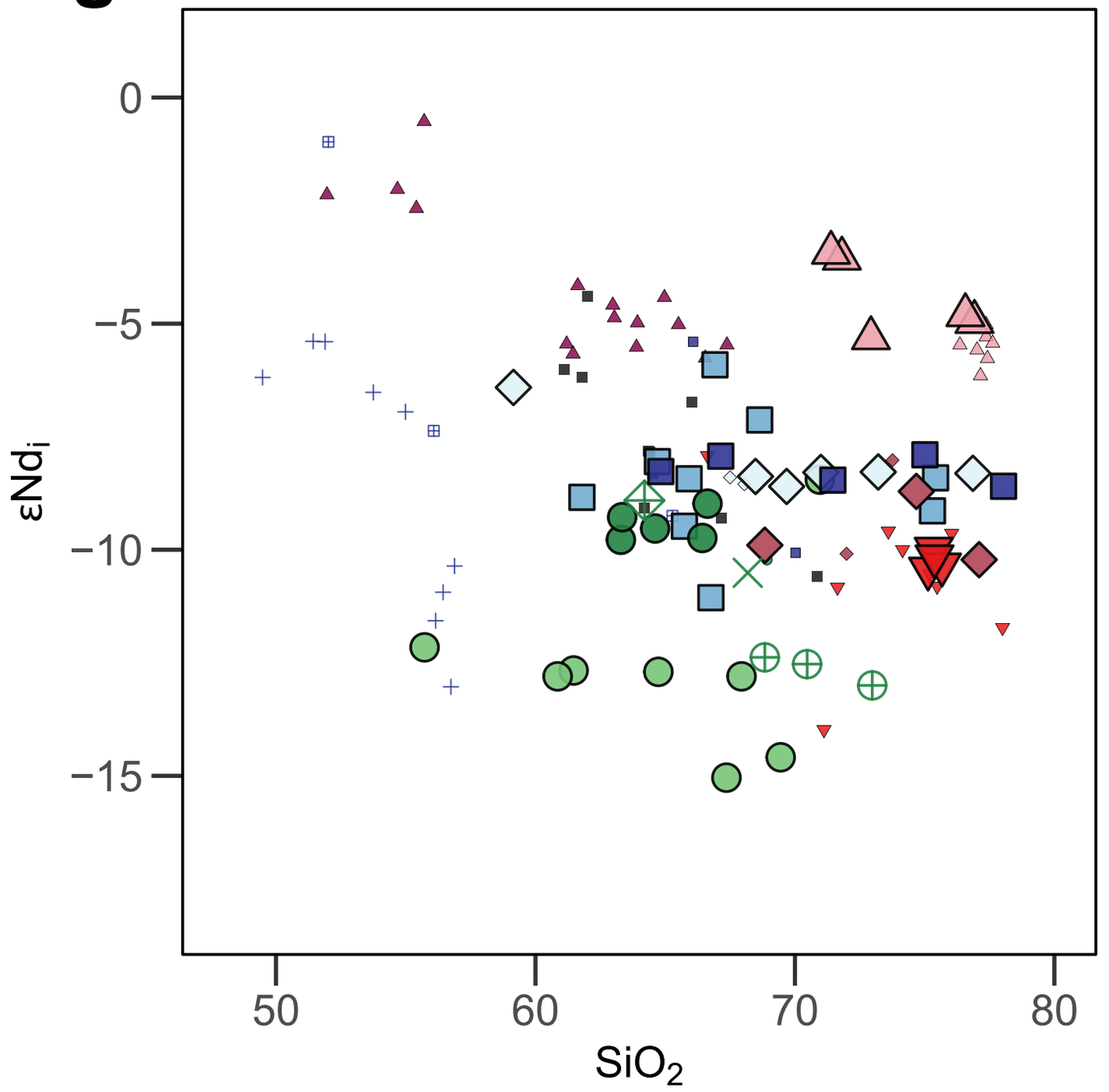

Figure 10

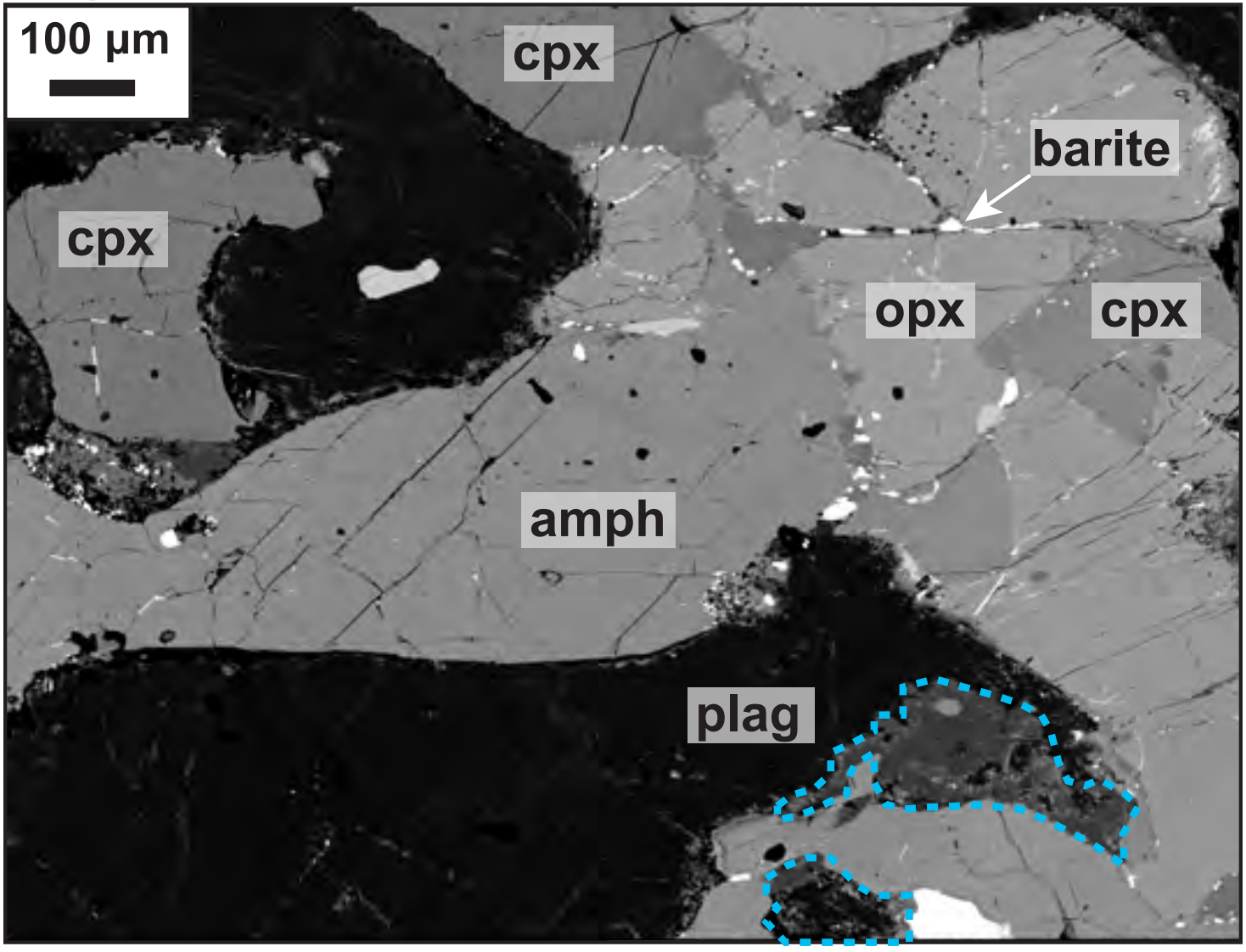

Figure 11

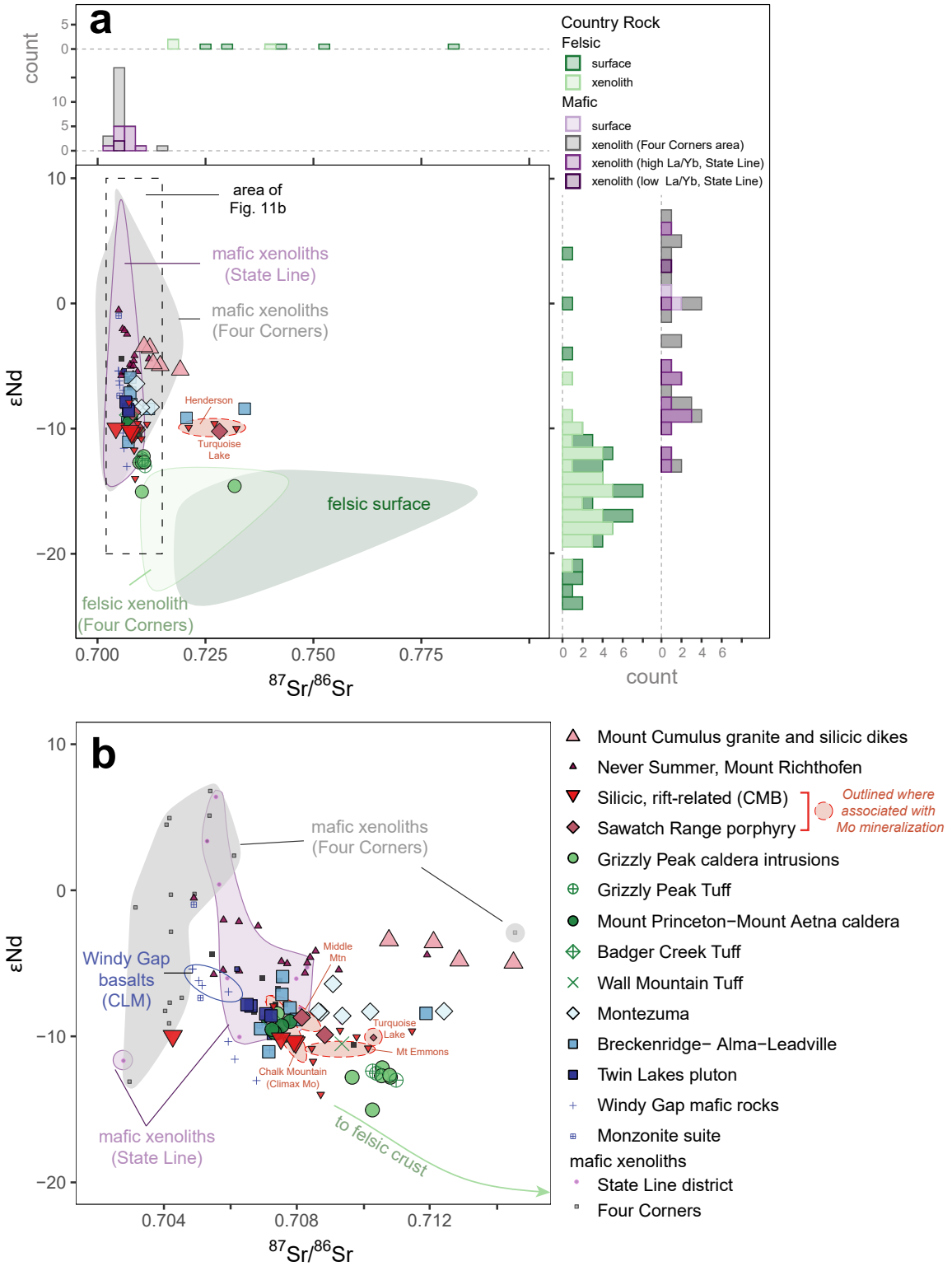
a
count
Country Rock
Felsic
surface
xenolith
Mafic
surface
xenolith (Four Corners area)
xenolith (high La/Yb, State Line)
xenolith (low La/Yb, State Line)
area of Fig. 11b
mafic xenoliths (State Line)
mafic xenoliths (Four Corners)
Henderson
Turquoise Lake
felsic surface
felsic xenolith (Four Corners)
εNd
87Sr/86Sr
count
b
mafic xenoliths (Four Corners)
Windy Gap basalts (CLM)
Middle Mtn
Turquoise Lake
Mt Emmons
Chalk Mountain (Climax Mo)
mafic xenoliths (State Line)
to felsic crust
Mount Cumulus granite and silicic dikes
Never Summer, Mount Richthofen
Silicic, rift-related (CMB)
Sawatch Range porphyry
Outlined where associated with Mo mineralization
Grizzly Peak caldera intrusions
Grizzly Peak Tuff
Mount Princeton–Mount Aetna caldera
Badger Creek Tuff
Wall Mountain Tuff
Montezuma
Breckenridge– Alma–Leadville
Twin Lakes pluton
Windy Gap mafic rocks
Monzonite suite
mafic xenoliths
State Line district
Four Corners

Figure 12

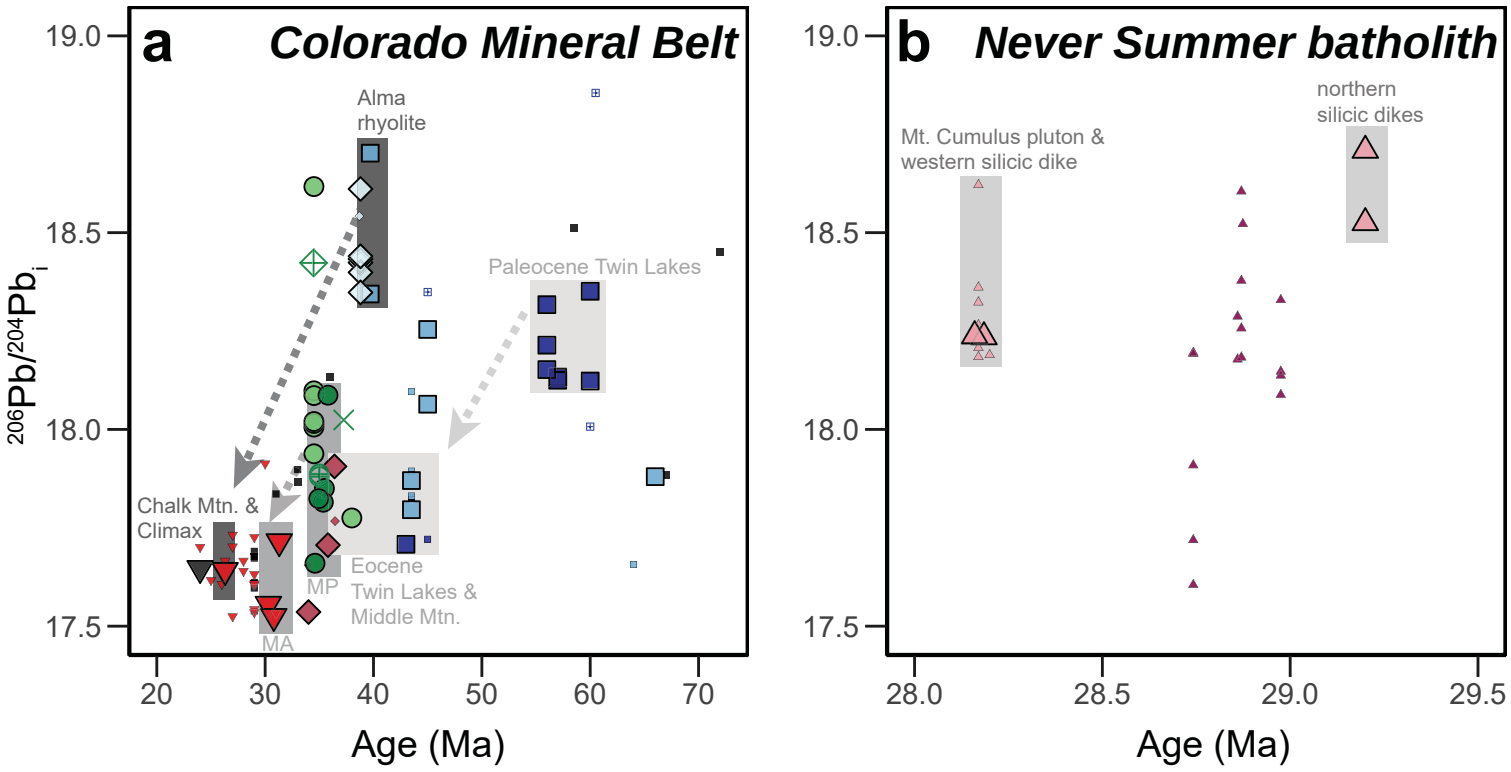
a
Colorado Mineral Belt
Alma
rhyolite
Paleocene Twin Lakes
Chalk Mtn. &
Climax
MP
Eocene
Twin Lakes &
Middle Mtn.
MA
19.0
18.5
18.0
17.5
$^{206}Pb/^{204}Pb_i$
20
30
40
50
60
70
Age (Ma)
b
Never Summer batholith
northern
silicic dikes
Mt. Cumulus pluton &
western silicic dike
19.0
18.5
18.0
17.5
28.0
28.5
29.0
29.5
Age (Ma)

Figure 13

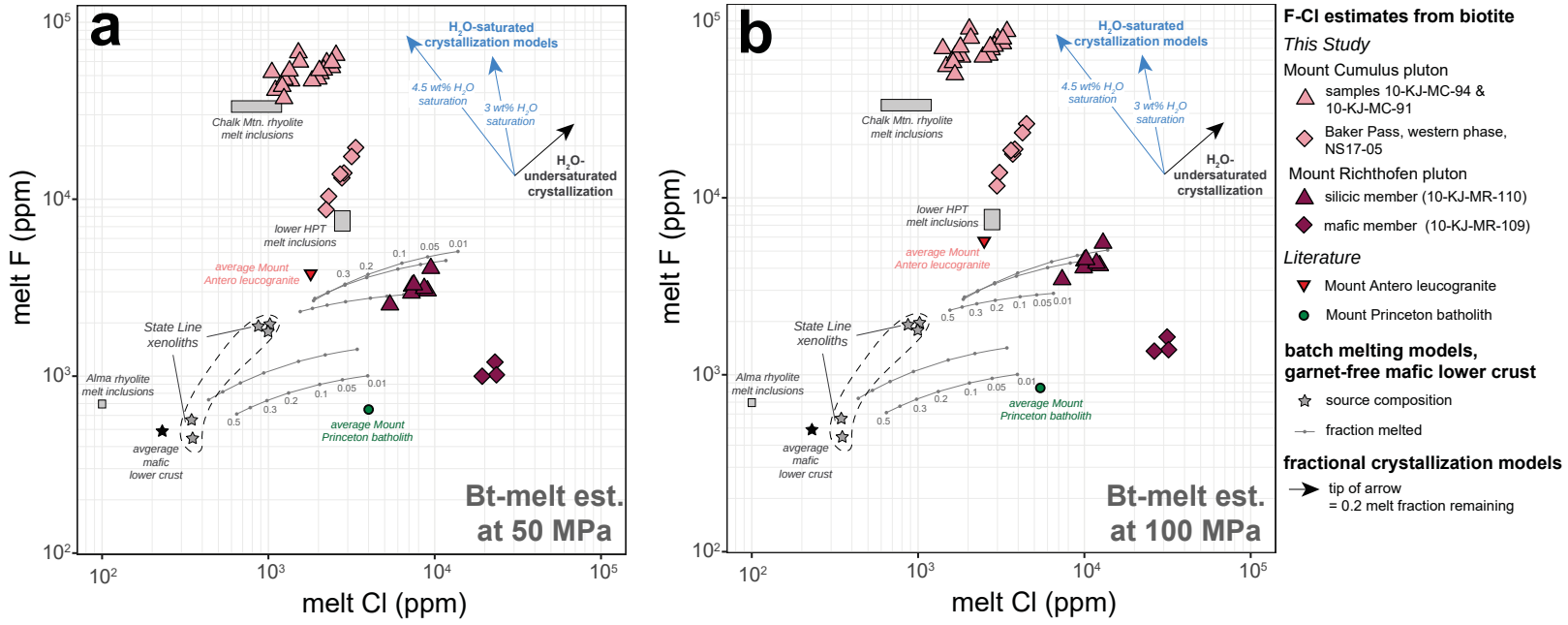
a
b
melt F (ppm)
melt Cl (ppm)
10^2
10^3
10^4
10^5
H_2O-saturated crystallization models
4.5 wt% H_2O saturation
3 wt% H_2O saturation
H_2O-undersaturated crystallization
Chalk Mtn. rhyolite melt inclusions
lower HPT melt inclusions
average Mount Antero leucogranite
State Line xenoliths
Alma rhyolite melt inclusions
avgerage mafic lower crust
average Mount Princeton batholith
0.5
0.3
0.2
0.1
0.05
0.01
Bt-melt est. at 50 MPa
Bt-melt est. at 100 MPa
F-Cl estimates from biotite
This Study
Mount Cumulus pluton
samples 10-KJ-MC-94 & 10-KJ-MC-91
Baker Pass, western phase, NS17-05
Mount Richthofen pluton
silicic member (10-KJ-MR-110)
mafic member (10-KJ-MR-109)
Literature
Mount Antero leucogranite
Mount Princeton batholith
batch melting models, garnet-free mafic lower crust
source composition
fraction melted
fractional crystallization models
tip of arrow = 0.2 melt fraction remaining

Figure 14

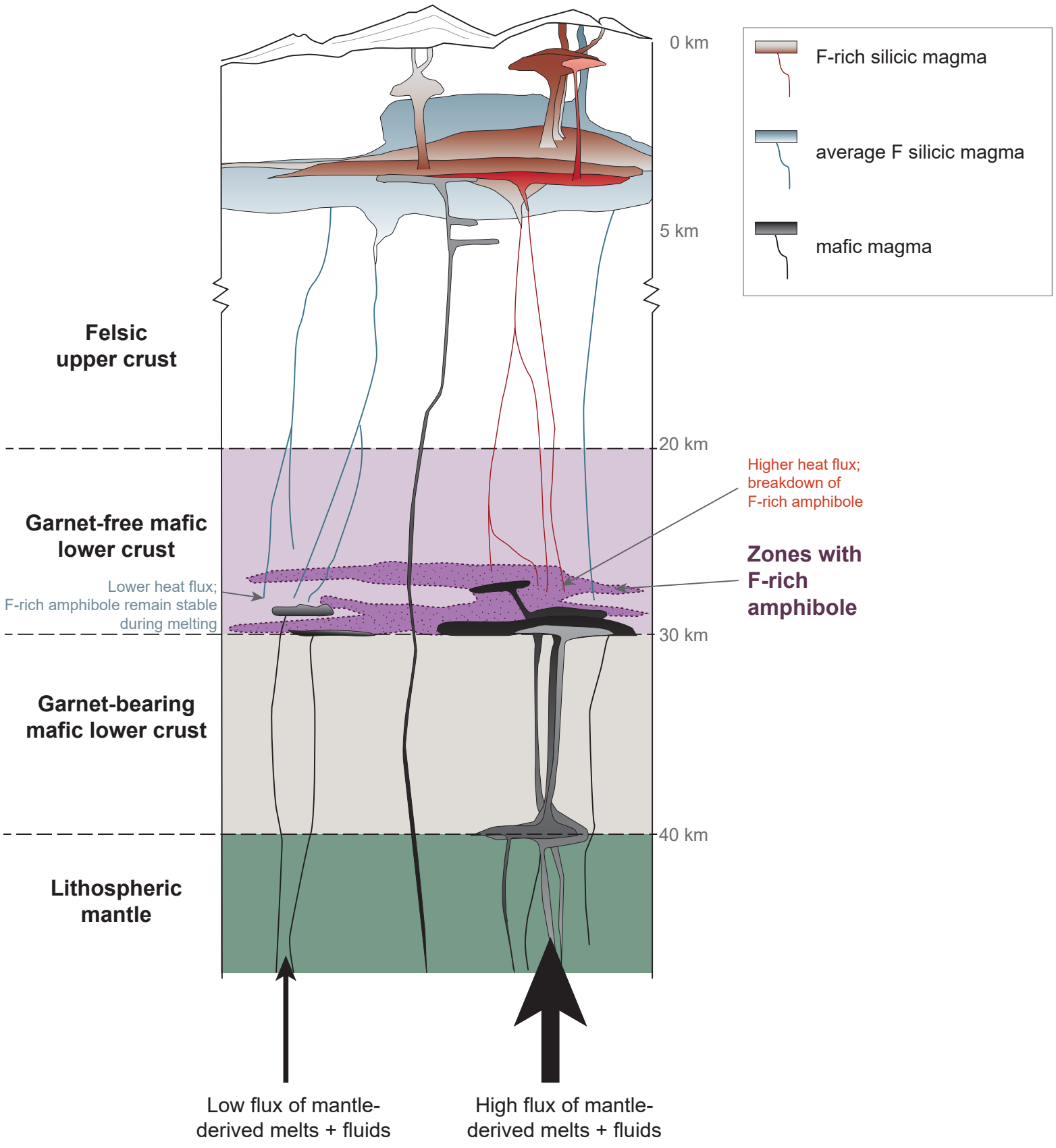
0 km
5 km
20 km
30 km
40 km
F-rich silicic magma
average F silicic magma
mafic magma
Felsic upper crust
Garnet-free mafic lower crust
Garnet-bearing mafic lower crust
Lithospheric mantle
Higher heat flux; breakdown of F-rich amphibole
Zones with F-rich amphibole
Lower heat flux; F-rich amphibole remain stable during melting
Low flux of mantle-derived melts + fluids
High flux of mantle-derived melts + fluids